The Canadian Mineralogist
Vol. 40, pp. 1347-1374 (2002)

CALCITE – AMPHIBOLE – CLINOPYROXENE ROCK FROM THE AFRIKANDA COMPLEX, KOLA PENINSULA, RUSSIA: MINERALOGY AND A POSSIBLE LINK TO CARBONATITES. III. SILICATE MINERALS

ANTON R. CHAKHMOURADIAN§

Department of Geological Sciences, University of Manitoba, 125 Dysart Road, Winnipeg, Manitoba R3T 2N2, Canada

ANATOLY N. ZAITSEV

Department of Mineralogy, St. Petersburg State University, 7/9 University Emb., St. Petersburg 199034, Russia

ABSTRACT

A calcite – amphibole – clinopyroxene rock (CAPR) occurs as veins and schlieren in cumulate ultramafic series of the Afrikanda complex, Kola Peninsula, Russia. The rock is composed of major amounts of diopside, amphibole, calcite, titanite, perovskite, magnetite and chlorite. Apart from xenocrysts derived from the ultramafic wallrocks, the Ti–Al–Mn-poor diopside (6–17 mol.% $NaFe^{3+}Si_2O_6$) and K–Ti-enriched magnesiohastingsite, with subordinate schorlomite and phlogopite, are the earliest minerals to crystallize. Their crystallization is believed to reflect the enrichment of a parental carbonatitic magma in silica (possibly, >40 wt.% SiO_2) and alkalis. The abundance of Na-bearing amphiboles and relative paucity of phlogopite reflect enrichment of the parental magma in Na relative to K. The early magnesiohastingsite is replaced and rimmed by sodic–calcic amphiboles, representing products of re-equilibration with a Na-rich carbothermal fluid. The fluid fractionated from the carbonatitic source was also enriched in *REE*, Nb and Th, as indicated by the replacement of early perovskite by loparite-(Ce) and ceroan lueshite. Separation of the fluid and associated fracturing were likely induced by decompression of partly crystallized carbonatitic magma. A series of replacement reactions observed in CAPR (perovskite ⇒ titanite, ilmenite ⇒ titanite and amphibole ⇒ chlorite) indicate a relatively high silica activity ($>10^{-4}$) and acidity of the fluid [$-\log a(H^+)$ well above the range –4 to –5.5]. The chlorite compositions, inferred to be in equilibrium with the fluid, yield temperatures near 200°C. The latest minerals to crystallize consist of zeolites, muscovite and prehnite that probably precipitated from a fluid derived from younger intrusions of foidolitic magma. The mode of occurrence and compositional variation of 23 silicate minerals identified in CAPR are presented and compared with the available data on other carbonatite complexes. A number of minerals described in this study [*e.g.*, gittinsite, cerite-(Ce) and calcium catapleiite] are either extremely rare or have not been previously reported to occur in carbonatites.

Keywords: clinopyroxene, amphibole, schorlomite, phlogopite, titanite, cerite-(Ce), chlorite, zircon, zirconosilicates, Ca–Al silicates, zeolites, carbonatite, Afrikanda, Kola Peninsula, Russia.

SOMMAIRE

Une roche à calcite – amphibole – clinopyroxene (CAPR) se présente sous forme de veines et de lentilles déformées dans la série de cumulats ultramafiques du complexe d'Afrikanda, dans la péninsule de Kola, en Russie. La roche contient des quantités importantes de diopside, amphibole, calcite, titanite, pérovskite, magnétite et chlorite. En plus des xénocristaux dérivés de l'encaissant ultramafique, le diopside à faible teneur en Ti, Al et Mn (6–17% $NaFe^{3+}Si_2O_6$, proportion molaire) et magnésiohastingsite enrichi en K et Ti, avec des quantités moindres de schorlomite et de phlogopite, sont les minéraux primaires précoces. Leur cristallisation reflèterait l'enrichissement du magma carbonatitique parental en silice (même peut-être plus de 40% SiO_2, poids) et en alcalins. L'abondance relative des amphiboles contenant le Na et la rareté de la phlogopite indiquent l'enrichissement du magma parental en Na plutôt qu'en K. La magnésiohastingsite précoce est entourée et remplacée par des amphiboles sodiques–calciques, produits d'un ré-équilibrage avec une phase fluide carbothermale riche en Na. La phase fluide émanant de la source carbonatitique était par surcroît enrichie en terres rares, Nb et Th, comme l'indique le remplacement de la pérovskite précoce par la loparite-(Ce) et la lueshite enrichie en cérium. La séparation de cette phase fluide et le développement de fissures associées résulteraient d'une décompression du magma carbonatitique partiellement cristallisé. Une série de réactions menant à des remplacements dans les roches CAPR (pérovskite ⇒ titanite, ilménite ⇒ titanite et amphibole ⇒ chlorite) indique une activité en silice relativement élevée ($>10^{-4}$) et une valeur d'acidité de la phase fluide [$-\log a(H^+)$] entre –4 et –5.5. Les compositions de chlorite, considérées avoir été en équilibre avec la phase fluide, indiquent une température voisine de 200°C. Parmi les minéraux tardifs se trouvent des zéolites, muscovite et prehnite, qui auraient précipité à partir d'une phase fluide dérivée

§ *E-mail address*: chakhmou@ms.umanitoba.ca

de venues intrusives de magma foïdolitique plus jeunes. Les aspects texturaux et la variation en composition des vingt-trois minéraux silicatés identifiés dans cette suite sont comparés avec les données disponibles d'autres complexes de carbonatite. Plusieurs minéraux signalés dans ce travail [*e.g.*, gittinsite, cérite-(Ce) et calcium catapléiite] sont rarissimes ou bien n'ont pas été décrits auparavant dans des carbonatites.

(Traduit par la Rédaction)

Mots-clés: clinopyroxène, amphibole, schorlomite, phlogopite, titanite, cérite-(Ce), chlorite, zircon, zirconosilicates, silicates de Ca–Al, zéolites, carbonatite, Afrikanda, péninsule de Kola, Russie.

Introduction

An unusual rock composed predominantly of calcic amphibole ("hornblende"), clinopyroxene and calcite was initially described at Afrikanda, southwestern Kola Peninsula, by Kupletskii (1938) and Kukharenko *et al.* (1965). This rock is developed primarily in the central part of that concentrically zoned intrusive body of ultramafic (clinopyroxenite with subordinate olivinite) and melteigite–urtitic rocks emplaced into the Precambrian metamorphic sequence of the Fennoscandian Shield. The geological setting and modal composition of the calcite – amphibole – clinopyroxene rock (hereafter, CAPR) were discussed in more detail in Chakhmouradian & Zaitsev (1999). In our previous studies, we demonstrated that the complex mineralogy of CAPR could not be explained in terms of simple fractionation of a silica-rich carbonatitic melt, and that the crystallization of CAPR involved subsolidus processes, as well as interaction of a parental liquid with the ultramafic wallrocks. The variety of oxide and carbonate phases found in CAPR provide important clues to the evolutionary history of this rock, including the late-stage enrichment of rare-earth elements in perovskite and zirconolite, oxygen-isotopic heterogeneity of calcite, occurrence of Na-carbonate inclusions in some rock-forming minerals, and variation in T and $f(O_2)$ throughout the late stages of crystallization (Chakhmouradian & Zaitsev 1999, Zaitsev & Chakhmouradian 2002). However, a detailed examination of silicate phases is clearly necessary for a critical assessment of the various genetic models proposed in the earlier studies. In the present work, we characterize the occurrence, interrelationships and compositional variation of silicate minerals from CAPR, and discuss implications of these mineralogical observations for the origin and crystallization history of carbonatitic rocks at Afrikanda. We also provide a detailed comparison of our data with those available in the literature for other carbonatite complexes. This comparison seems both appropriate and timely, because, with the exception of amphiboles (Hogarth 1989), no such assessment has been undertaken since the publication of Kapustin's (1971) monograph on the mineralogy of carbonatites. Compositional data for many important silicate minerals from carbonatitic rocks (*e.g.*, garnets, titanite and chlorite) are limited to a few analyses, and are rarely considered in a petrogenetic context.

Analytical Methods

The composition of all minerals was determined by energy-dispersion X-ray spectrometry (EDS) using a Hitachi 570 scanning electron microscope equipped with a LINK ISIS analytical system. Raw EDS spectra were acquired for 100–180 seconds (live time) with an accelerating voltage of 20 kV and a beam current of 0.54–0.55 nA. The spectra were processed using the LINK ISIS SEMQUANT software package, with full ZAF corrections applied. The following standards were used: benitoite (Ba), corundum (Al), manganoan fayalite (Mn), fluorapatite (P), ilmenite (Fe and Ti), jadeite (Na), loparite-(Ce) (La, Ce, Pr, Nd and Nb), orthoclase (K), wollastonite (Ca and Si), synthetic $SrTiO_3$ (Sr), SmF_3 (Sm), metallic Zr, Hf and Th. The composition of the Zr silicates, which contain elements with strongly overlapping analytical lines, was also examined by wavelength-dispersion X-ray spectrometry (WDS) using a CAMECA SX–50 electron microprobe operated at 15 kV and 20 nA. The following standards were employed for the WDS analysis: albite (Na), diopside (Ca), fayalite (Fe), forsterite (Mg), kyanite (Al), titanite (Ti), synthetic $ZrSiO_4$ (Zr and Si), $HfSiO_4$ (Hf), ThO_2, UO_2 and $MnNb_2O_6$ (Nb).

X-ray powder-diffraction (XRD) patterns of selected minerals were obtained using a Philips 3710 diffractometer (Cu$K\alpha$ radiation) operated at 30 mA and 40 kV, in a step-scanning mode with a step size of 0.02–0.04°2θ. The unit-cell parameters were calculated from XRD data using the UnitCell software (Holland & Redfern 1997), which utilizes a non-linear least-squares method.

Silicate Minerals: Parageneses and Compositions

Primary paragenesis

Clinopyroxene is the principal constituent of CAPR, locally comprising up to 80 vol.% of the rock. This mineral forms elongate prismatic crystals of dark dirty-green color up to several cm in length. The crystals are locally resorbed and replaced by calcic amphibole and calcite along the rim and fractures (Fig. 1). In thin section, this clinopyroxene is pale green and very weakly pleochroic. Samples from the contact of CAPR with the ultramafic suite also contain fine-grained xenocrysts of

golden yellow, distinctly pleochroic clinopyroxene identical to that occurring in the wallrock clinopyroxenite. The xenocrysts show replacement textures similar to those described above. It is noteworthy that we did not observe rimming or replacement of the xenocrystic clinopyroxene by the later-crystallized pale green variety; occasional xenocrysts embedded in the pale green clinopyroxene are not in optical continuity with the host. In addition to the yellowish relict pyroxene, the near-contact zones of CAPR contain abundant xenocrysts of brownish yellow perovskite (Fig. 1a) and titaniferous magnetite.

In terms of chemical composition, the pale green clinopyroxene corresponds to Ti-, Al- and Mn-poor diopside (Table 1, anal. 1–4). The Na content is variable, but systematically exceeds 0.8 wt.% Na_2O (~ 6 mol.% $NaFe^{3+}Si_2O_6$, *Ae*), increasing locally along the rim to 17 mol.% *Ae*. This diopside is compositionally distinct from the relict yellowish clinopyroxene, which is enriched in Al and Ti (2.2–3.6 and 1.4–1.9 wt.% respective oxides), but comparatively poorer in Na (<0.6 wt.% Na_2O or 4 mol.% *Ae*) and Mn (typically, below detection). The Al–Ti enrichment is characteristic of clinopyroxenes from the ultramafic suites (*cf.* Table 1, anal. 5–7), The representative compositions of the Afrikanda diopside are shown in Figure 2, and compared with clinopyroxene from other occurrences. The compositions of the pale green crystals are closest to diopside from the Maimecha–Kotuy phoscorites and Loch Borralan carbonatite intrusion in Scotland, although the latter was interpreted as xenocrystic and derived from associated mafic rocks (Young *et al*. 1994). Other available compositions comprise an ill-defined trend toward more Fe-rich compositions, with the examples from the Fen "silicocarbonatite" being the richest in Na and Fe^{3+}, *i.e*. most evolved (up to 27 mol.% *Ae*: Mitchell 1980).

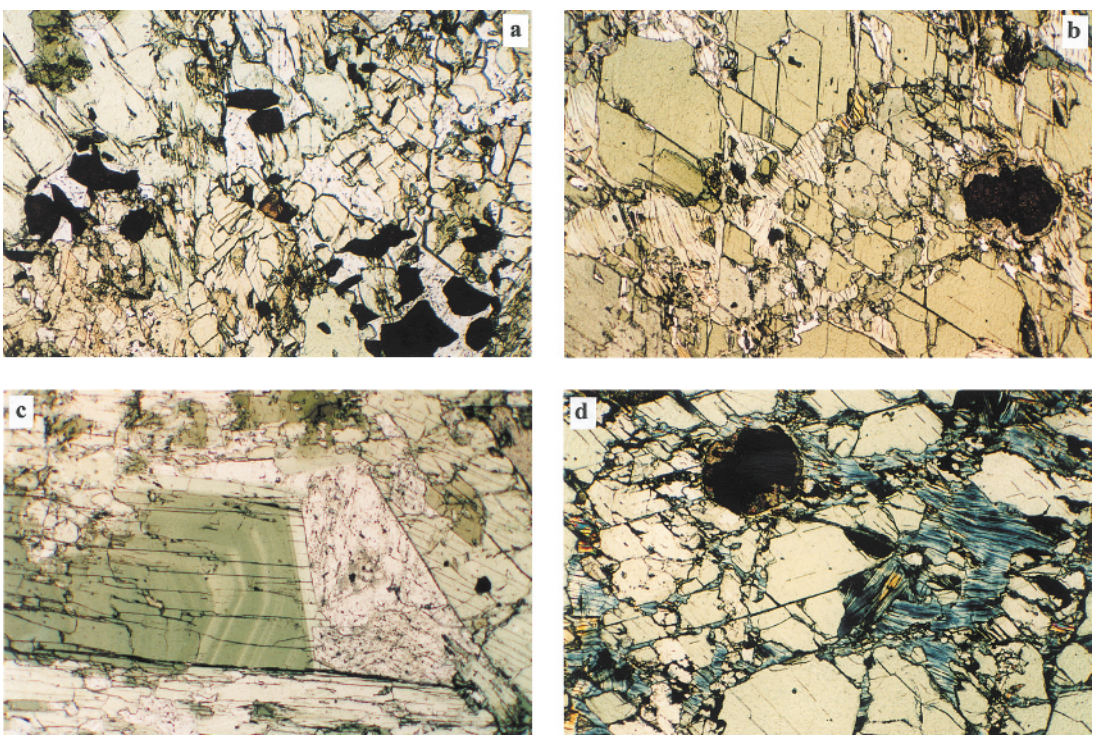

FIG. 1. Photomicrographs of some characteristic textures observed in silicate-rich portions of CAPR. (a) Fractured xenocrystic clinopyroxene (yellowish grain in the center) surrounded by pale green diopside; other minerals are xenocrystic perovskite (dark brown, center), magnetite (opaque), calcite (colorless) and magnesiohastingsite replacing the clinopyroxene (green to light yellow); (b) magnesiohastingsite (yellowish green) successively replaced by magnesiokatophorite plus richterite (lighter colored, more grayish) and clinochlore (colorless) along fractures; also note perovskite crystal (dark brown) replaced by titanite along the rim; (c) oscillatory-zoned magnesiohastingsite with a richterite rim (lighter-colored); the pale green mineral partly replaced by amphibole is diopside, and the colorless material is primary calcite; (d) replacement of the amphiboles (pale green) by clinochlore (anomalous interference-colors). (a)–(c) Plane-polarized light, (d) crossed polars; width of the field of view is 5.5 mm for all images.

More recent studies show that sövite from the same locality contains sodic clinopyroxene with 37–98 mol.% *Ae* (Andersen 1988). Notably, aegirine has been identified in a number of other carbonatite intrusions (*e.g.*, Brazil Branch in Arkansas: McCormick & Heathcote 1987), but analytical data for this mineral are typically lacking. In common with the pale green crystals from CAPR, most carbonatites contain clinopyroxene poor in Al (<0.10 atoms per formula unit, *apfu*), the two noteworthy exceptions being the Arkansas group of intrusions (up to 0.38 *apfu* Al: McCormick & Heathcote 1987) and the Newania complex in India (Viladkar & Wimmenauer 1986). Aluminous clinopyroxene from the latter locality was considered xenocrystic.

Garnet-group minerals crystallized throughout the evolutionary history of CAPR, and are represented by three major types differing in both morphology and chemistry. The earliest type to crystallize consists of pitch-black subhedral to euhedral crystals intimately associated with magnesiohastingsite. The crystals do not exceed 3 cm in diameter, and exhibit {110} faces as the only recognizable form. The mineral is brownish red in thin section, and shows no significant variation in color within the crystal. Compositionally, this is a granditic garnet, with very high Ti contents (14.2–16.8 wt.% TiO_2), and significant levels of Mg, Zr and Na (Table 1, anal. 8–10). Following the somewhat arbitrary criteria

TABLE 1. REPRESENTATIVE COMPOSITIONS OF CLINOPYROXENE AND GARNET

Wt.%	1	2	3	4	5	6	7		8	9	10	11	12
	CLINOPYROXENE								GARNET				
Na_2O	1.20	1.62	1.95	2.42	0.38	0.67	0.45		0.08	0.17	0.47	0.28	n.d
CaO	23.29	22.15	22.17	21.25	24.78	24.01	24.17		31.65	32.12	31.58	32.25	32.66
MgO	15.45	14.50	14.50	14.47	15.23	13.57	14.80		1.34	1.33	1.16	0.64	0.42
MnO	0.09	0.16	0.17	0.21	n.d	0.08	0.05		0.13	0.31	0.33	0.22	0.09
FeO	2.31	1.93	1.89	-	1.15	1.05	1.12		2.85	4.15	4.63	1.04	1.17
Fe_2O_3	3.18	4.28	5.17	7.12	3.86	5.72	4.35		17.87	15.17	15.14	24.48	26.36
TiO_2	0.18	0.07	0.19	0.07	1.84	2.16	1.56		14.15	15.68	16.79	7.48	4.41
ZrO_2	n.d	n.d	n.d	n.d	n.d	n.d	n.d		1.67	1.78	2.22	1.32	n.d
Al_2O_3	0.38	0.14	0.25	0.26	2.94	4.90	3.29		2.35	2.59	1.04	1.04	0.75
SiO_2	54.57	53.33	54.52	53.82	50.31	47.88	49.52		27.38	28.27	27.99	31.44	33.43
Total	100.65	98.18	100.81	99.62	100.49	100.04	99.31		99.47	101.57	101.35	100.19	99.29
Structural formulae calculated on the basis of:													
	6 atoms of oxygen								12 atoms of oxygen				
Na	0.085	0.117	0.138	0.173	0.027	0.048	0.032	Na	0.013	0.028	0.077	0.046	-
Ca	0.908	0.887	0.866	0.838	0.974	0.955	0.962	Ca	2.898	2.872	2.851	2.927	2.974
Σ	0.993	1.004	1.004	1.011	1.001	1.003	0.994	Mg	0.080	0.078	0.048	0.011	0.020
								Mn	0.009	0.022	0.024	0.016	0.006
								Σ	3.000	3.000	3.000	3.000	3.000
Mg	0.838	0.809	0.788	0.794	0.833	0.751	0.820	Mg	0.091	0.087	0.098	0.070	0.033
Mn	0.003	0.005	0.005	0.007	-	0.003	0.002	Mn	-	-	-	-	-
Fe^{2+}	0.072	0.060	0.058	-	0.035	0.033	0.035	Fe^{2+}	0.214	0.301	0.340	0.078	0.089
Fe^{3+}	0.087	0.120	0.140	0.188	0.080	0.150	0.105	$Fe^{3+}{}_{VI}$	0.716	0.556	0.407	1.321	1.596
Ti	0.005	0.002	0.005	0.002	0.051	0.060	0.044	Ti	0.909	0.984	1.064	0.476	0.282
Zr	-	-	-	-	-	-	-	Zr	0.070	0.072	0.091	0.055	-
Al_{VI}	0.002	-	-	-	-	-	-	Al_{VI}	-	-	-	-	-
Σ	1.007	0.996	0.996	0.991	0.999	0.997	1.006	Σ	2.000	2.000	2.000	2.000	2.000
Al_{IV}	0.014	0.006	0.011	0.011	0.127	0.214	0.144	Al_{IV}	0.237	0.256	0.103	0.104	0.075
$Fe^{3+}{}_{IV}$	-	-	0.002	0.009	0.027	0.009	0.016	$Fe^{3+}{}_{IV}$	0.423	0.385	0.539	0.233	0.084
Si	1.986	1.994	1.987	1.980	1.846	1.777	1.840	Si	2.340	2.359	2.358	2.663	2.841
Σ	2.000	2.000	2.000	2.000	2.000	2.000	2.000	Σ	3.000	3.000	3.000	3.000	3.000

Compositions: 1-4 diopside from CAPR; 5 xenocrystic aluminian diopside derived from clinopyroxenite; 6-7 aluminian diopside from clinopyroxenite; 8-10 primary schorlomite from CAPR; 11-12 core and rim of an andradite overgrowth on schorlomite from CAPR. All data this work. Fe^{2+}/Fe^{3+} ratio estimated from stoichiometry; n.d = not detected.

of Howie & Woolley (1968), the Afrikanda garnet may be classified as schorlomite (>0.5 *apfu* Ti to 12 atoms of oxygen). In common with Ti-bearing garnets from other localities, those from Afrikanda show a deficit of Si in the tetrahedral site (20–23% of the total occupancy).

The crystal chemistry of schorlomite and related phases has been scrutinized in numerous studies, but there is still no complete agreement among mineralogists as to the distribution of different cations among the six- and four-coordinated sites. In most studies, Ti in the garnet structure is interpreted as tetravalent and present exclusively in the octahedra (*e.g.*, Amthauer *et al.* 1977, Locock *et al.* 1995). In such a case, the incorporation of Ti^{4+} must be accompanied by substitution of the proportional amount of Si by lower-valence cations, *i.e.*, Fe^{3+} plus subordinate Fe^{2+} (Kühberger *et al.* 1989, Locock *et al.* 1995, Armbruster *et al.* 1998), or predominantly Al^{3+} (Müntener & Hermann 1994). The significance of $Si^{4+} \Leftrightarrow Al^{3+}$ substitution is believed to increase in Zr-enriched schorlomite owing to structural constraints (Armbruster *et al.* 1998). Using elemental correlations, Dingwell & Brearley (1985) and Lupini *et al.* (1992) argued for the presence of significant tetrahedral Ti^{4+} and Zr^{4+}, respectively. However, the replacement of Si^{4+} by Zr^{4+} seems highly unlikely because of the large difference in size between these cations. The compositional complexity of Ti-bearing garnets may be further affected by the presence of Ti^{3+} and $(O_4H_4)^{4-}$ groups that are incorporated into the octahedral and tetrahedral sites, respectively (Wu & Mu 1986, Malitesta *et al.* 1995, Armbruster *et al.* 1998).

The crystal structure of a representative sample of the Afrikanda schorlomite was refined by single-crystal methods (Chakhmouradian & Cooper, unpubl. data), and proved to be undistorted and cubic (space group *Ia3d*). The interatomic distances determined from the structural data suggest that the tetrahedral site incorporates not only Fe^{3+} and Si^{4+}, but also a cation of intermediate size, possibly Al^{3+}. The Ca–(Ti,Fe) distance, corrected for the grossular component (for details, see Armbruster *et al.* 1998), is 1.399 Å. On their Ca–(Ti,Fe) *versus* Ti diagram, this distance corresponds to *ca.* 1.0 *apfu* Ti; exactly the same value was calculated from the average result of 15 electron-microprobe analyses. The excellent correspondence between the two values rules out the presence of significant Ti^{3+} in our schorlomite, because this would have resulted in an anomalously short Ca–(Ti,Fe) distance and cell parameter (*cf.* data for morimotoite: Henmi *et al.* 1995). Hence, the compositions of the Afrikanda schorlomite were recalculated to structural formulae on the basis of 8 cations and 12 atoms of oxygen, with all Ti cast as Ti^{4+}. We also neglected the possible presence of minor H_2O in our samples, as the $(SiO_4)^{4-} \Leftrightarrow (O_4H_4)^{4-}$ substitution has very limited significance in schorlomite (Armbruster *et al.* 1998).

At the contact with calcite and chlorite, the primary schorlomite is normally surrounded by a thin discontinuous rim of brownish yellow color. Both schorlomite

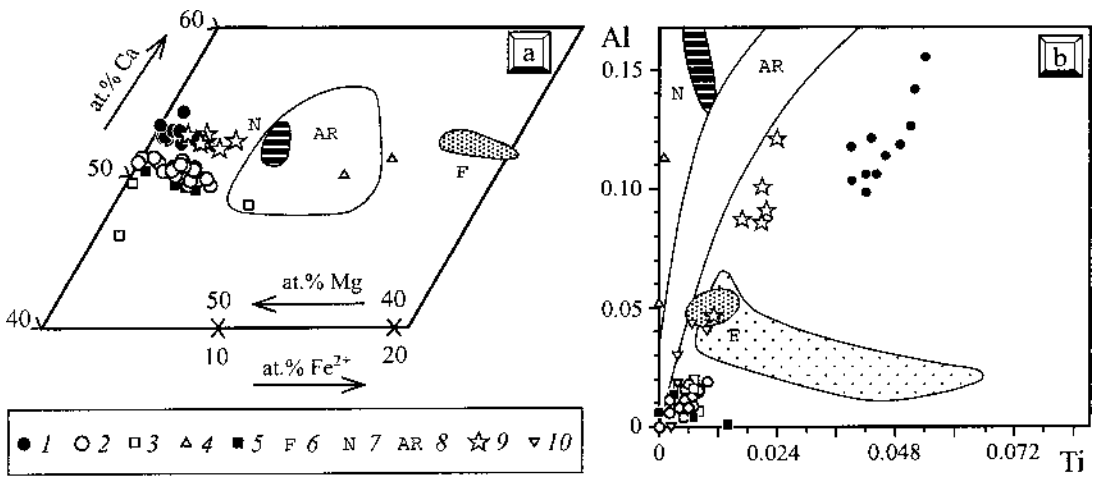

FIG. 2. Compositional variation of clinopyroxene from Afrikanda (1 ultramafic rocks, 2 CAPR), and other carbonatite and phoscorite occurrences, including the Maimecha–Kotuy Province in Siberia (3), In'Ouzzal in Algeria (4), Loch Borralan in Scotland (5), Fen in Norway (6), Newania in India (7), the Arkansas group of intrusions (8), Gornoe Ozero in Siberia (9), and Turiy Mys in Kola (10). (a) Ca–Mg–Fe^{2+} (at.%) diagram, (b) Al *versus* Ti (*apfu*) diagram. The diagram was constructed using the data of Mitchell (1980), Viladkar & Wimmenauer (1986), McCormick & Heathcote (1987), Andersen (1988), Ouzegane *et al.* (1988), Egorov (1991), Bagdasarov (1994), Young *et al.* (1994), and authors' unpublished data.

and the rim are locally replaced by titanite. Where the titanite alteration is absent, the rim appears to consist of coalescent bulbous overgrowths up to 0.5 mm across. Within these overgrowths, the intensity of color invariably decreases outward, in parallel with the diminishing Ti content (Table 1, anal. 11–12). This generation of garnet (type 2) contains <0.5 *apfu* Ti, and should be termed titanian andradite. The Ti-bearing garnets from CAPR show an overall evolutionary trend of decreasing (Ti + Zr), Al and Mg, and increasing Fe^{3+} contents, although some compositions deviate from the major trend toward lower Al values (Fig. 3). Poor correlation between the Ca and Mg contents indicates that Mg enters not only the Ca site, but also the octahedral site, as suggested previously by Locock *et al.* (1995, p. 34) and other investigators.

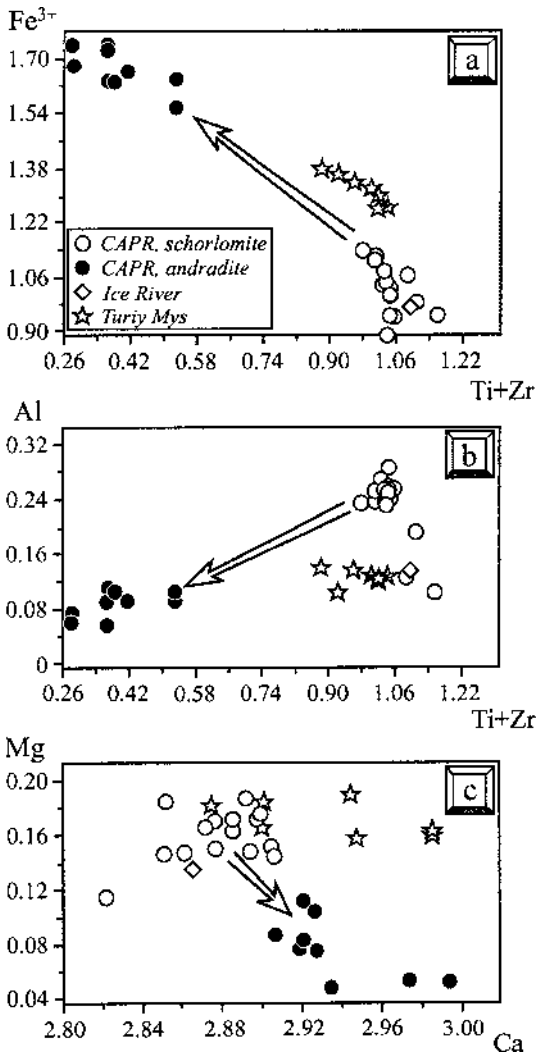

FIG. 3. Variation of major components (*apfu*) in the composition of titanian garnets from CAPR. The compositions of schorlomite from Ice River melteigite (Locock *et al.* 1995) and Turiy Mys turjaite (authors' unpubl. data) are plotted for comparison.

Titanian garnets are common in diverse petrographic settings (carbonatites, alkali syenites, contact-metamorphic assemblages, melilitolites, foidolites and foidites), but it is difficult to delineate compositional traits characteristic of a specific rock-type. For example, the Afrikanda material is very similar in terms of its major- and minor-element contents to schorlomite from the Ice River melteigite (Canada) and Turiy Mys turjaite (Russia) (Fig. 3). Generally speaking, schorlomite from carbonatites and melilitic rocks has elevated levels of Zr, but the Zr content may vary significantly both within individual crystals and among different petrographic units (Platt & Mitchell 1979, Lupini *et al.* 1992, Ulrych *et al.* 1994).

The latest generation of garnet to crystallize (type 3) is represented by ferrian hibschite, $Ca_3(Al,Fe)_2(SiO_4)_{3-x}(OH)_{4x}$, whose occurrence is restricted to the late-stage calc-silicate paragenesis, and will be discussed in detail below.

Phlogopite is present in CAPR in minor amounts, and invariably in association with magnetite. This phlogopite shows normal absorption ($Z > X$), and pleochroism from colorless or pale yellow to olive-green. The mineral is characterized by a low Fe/(Mg + Fe) value (*ca.* 0.2), elevated levels of Na (>0.12 *apfu*), and moderate Ba and Ti contents (Table 2, anal. 1–2). Phlogopite also occurs as a "corona" around magnetite crystals in the wallrock clinopyroxenites; however, its composition is comparatively enriched in Mg, Ti and Na, indicating somewhat different conditions of crystallization.

Ferromagnesian trioctahedral micas are probably the most common (and best studied) silicate minerals in carbonatitic rocks. They occur as macro-, pheno- and oikocrysts, cumulates, and reaction-induced rims on macrocrysts (xenocrysts) of other ferromagnesian minerals. The micas also develop at the contact of carbonatite bodies with ultramafic and alkaline wallrocks, ranging in scale from a thin incrustation of isolated crystals to a massive zone of "glimmerite" (*e.g.*, Morbidelli *et al.* 1986, Young *et al.* 1994). Irrespective of the mode of occurrence, most of these micas represent relatively Mg-rich members of the "biotite" (phlogopite – annite – tetra-ferriphlogopite) series. To the best of our knowledge, only carbonatites and phoscorites from Khibina (Kola Peninsula) have been reported to contain micas with a preponderance of Fe over Mg in the octahedral positions [Fe/(Mg + Fe) up to 0.66] (Zaitsev 1992). The compositional variation of "biotite" from different carbonatite occurrences can be conveniently illustrated using the [4 – (Si + Al)] *versus* Fe/(Mg + Fe) diagram (Figs. 4a, b: modified after McCormick & Le Bas 1996). Typically, these micas

TABLE 2. REPRESENTATIVE COMPOSITIONS OF PHLOGOPITE AND AMPHIBOLE

Wt.%	1	2	3	4	5	6	7	8	9	10
	PHLOGOPITE		AMPHIBOLE							
Na_2O	1.03	0.96	2.94	3.27	6.71	7.43	4.01	4.59	4.15	7.56
K_2O	8.42	8.35	1.10	1.18	0.47	0.29	0.70	0.52	0.70	0.35
CaO	n.d	n.d	12.87	12.07	7.34	6.23	11.58	10.72	11.28	6.46
BaO	0.76	2.11	n.a	n.a	n.a	n.a	n.a	n.a	n.a	n.a
MgO	22.55	21.47	15.37	15.43	17.95	19.64	16.72	18.01	16.92	20.70
MnO	0.35	0.24	0.28	0.22	0.06	0.17	0.17	0.06	0.20	0.24
FeO	6.15	9.02	7.56	5.80	5.75	3.61	6.49	5.55	5.10	3.82
Fe_2O_3	3.59	0.96	4.36	6.31	4.64	4.65	4.03	2.24	6.23	2.74
TiO_2	1.35	0.86	1.32	1.26	1.30	0.68	1.49	1.16	1.54	0.68
Al_2O_3	13.59	12.75	11.99	11.68	4.87	1.88	9.29	7.35	9.61	1.18
SiO_2	38.48	38.42	42.42	41.09	49.53	53.36	44.33	45.87	44.65	55.01
Total	96.27	95.14	100.21	98.31	98.62	97.94	98.81	96.07	100.38	98.74
Structural formulae calculated on the basis of:										
	11 atoms of oxygen		23 atoms of oxygen							
Na	0.144	0.138	0.821	0.927	1.846	2.031	1.121	1.298	1.144	2.035
K	0.773	0.788	0.202	0.220	0.085	0.052	0.129	0.096	0.127	0.062
Ca	-	-	1.984	1.892	1.116	0.941	1.787	1.676	1.719	0.961
Ba	0.021	0.061	-	-	-	-	-	-	-	-
Σ	0.938	0.987	3.007	3.039	3.047	3.024	3.037	3.070	2.990	3.058
Mg	2.419	2.369	3.297	3.366	3.798	4.130	3.593	3.918	3.588	4.284
Mn	0.021	0.015	0.034	0.027	0.007	0.020	0.021	0.007	0.024	0.028
Fe^{2+}	0.371	0.559	0.908	0.709	0.551	0.425	0.783	0.677	0.606	0.444
$Fe^{3+}{}_{VI}$	0.116	0.009	0.473	0.696	0.459	0.329	0.404	0.201	0.627	0.115
Ti	0.073	0.048	0.143	0.139	0.138	0.072	0.162	0.127	0.165	0.071
Al_{VI}	-	-	0.138	0.024	-	-	-	-	-	-
Σ	3.000	3.000	4.993	4.961	4.953	4.976	4.963	4.930	5.010	4.942
$Fe^{3+}{}_{IV}$	0.078	0.044	-	-	0.156	0.165	0.033	0.045	0.039	0.171
Al_{IV}	1.153	1.112	1.896	1.990	0.815	0.312	1.578	1.264	1.611	0.193
Si	2.769	2.844	6.104	6.010	7.029	7.523	6.389	6.691	6.350	7.636
Σ	4.000	4.000	8.000	8.000	8.000	8.000	8.000	8.000	8.000	8.000

Compositions: 1-2 weakly zoned crystal of phlogopite enclosed in magnetite; 3-6 magnesiohastingsite replaced by richterite and chlorite (Fig. 1b); 7-10 oscillatory-zoned crystal of amphibole (Fig. 1c): magnesiohastingsite core (7), intermediate low-AZ zone (8), intermediate high-AZ zone (9), and richterite rim (10). All data this work. Fe^{2+}/Fe^{3+} ratio estimated from stoichiometry; n.d = not detected; n.a = not analyzed.

show an evolutionary trend of decreasing Al and increasing Fe^{3+} content, generally accompanied by a transition from phlogopite to tetra-ferriphlogopite (*e.g.*, Basu & Mayila 1986, Middlemost 1990, Young *et al.* 1994). A similar trend was documented for alkali-ultramafic pegmatites of the Kovdor intrusion in Kola (Krasnova 2001). A distinctly reverse trend involving an increase in ^{IV}Al has been thus far observed only in phlogopitic–eastonitic micas from the Arkansas carbonatites (McCormick & Heathcote 1987) and in one sample from Sarfartôq, Greenland (Secher & Larsen 1980). The interpretations provided by McCormick & Heathcote in the text (1987, p. 61) need verification, as they are at variance with the data included in their Table 2. The zoning toward more aluminous compositions in the Sarfartôq phlogopite was explained by contamination of the host carbonatite with wallrock material (Secher & Larsen 1980). Where the chemical evolution of mica can be traced from antecedent ultramafic rocks to carbonatites, it also involves enrichment in Fe^{3+} coupled with decreasing proportion of Ti and Fe^{2+} in the octahedral site (Skosyreva *et al.* 1988, Brigatti *et al.* 1996). Cocrystallization of mica with competitor Fe–Mg phases, and contamination of carbonatitic magma with silicate rocks, may result in more complex compositional patterns, as inferred by McCormick & Le Bas (1996) for the Ugandan complexes (Fig. 4a).

Micas from carbonatites exhibit a significant range in Na and Ba contents (Fig. 4c). A core-to-rim variation in Ba has been described in phlogopite crystals from some occurrences, and may involve either increase or decrease in the amount of Ba (Gaspar & Wyllie 1982, Reguir 2001, respectively). The phlogopite from CAPR is compositionally similar to micas from a number of carbonatite occurrences worldwide (Fig. 4 and references therein), but lacks any consistent intragranular variation in Fe or Al content; some crystals exhibit narrow inner zones subtly enriched in Ba (Table 2, anal. 2).

Amphiboles account for up to 20% of CAPR by volume. The earliest type of amphibole forms coarse prismatic crystals of greenish black color and anhedral grains replacing the diopside (Fig. 1a). In thin section, this type is pleochroic from nearly colorless (*X*) to pinkish yellow (*Y*) to brownish green (*Z*). Many crystals are fractured, fragmented and altered to chlorite along their rim and fractures. This amphibole is devoid of primary zoning, but contains lighter-colored areas typically associated with patches of chlorite (Fig. 1b); in back-scattered electron (BSE) images, these areas have a lower average atomic number (AZ) owing to their enrichment in Na and Mg relative to the bulk of the crystals. In transmitted light, the late-stage amphibole ranges from almost colorless to pale green with a distinct bluish hue, absent in the early-formed type. Calcite-filled interstices between the diopside laths are commonly incrusted with small (a few mm in length) euhedral crystals of amphibole showing an oscillatory pattern of zoning (Fig. 1c). The observed variation in color reflects changes in the Fe/Mg value across the crystal. The rim of oscillatory-zoned amphibole is optically and chemically similar to the pale-colored areas within the large crystals.

The primary amphibole is essentially homogeneous in composition, and corresponds to K–Ti-enriched (*ca.* 0.20 *apfu* K, 0.15 *apfu* Ti) magnesiohastingsite (Table 2, anal. 3–4). The oscillatory-zoned crystals also correspond to magnesiohastingsite, but differ from the large crystals in having noticeably lower K, Ca, Fe and Al contents (Table 2, anal. 7–9). The pale green zones have lower levels of Fe, Al, K and, to some extent, Ti, in comparison with the darker-colored zones. The low-AZ areas correspond predominantly to richterite (Table 2, anal. 6, 10); a few compositions have intermediate Al

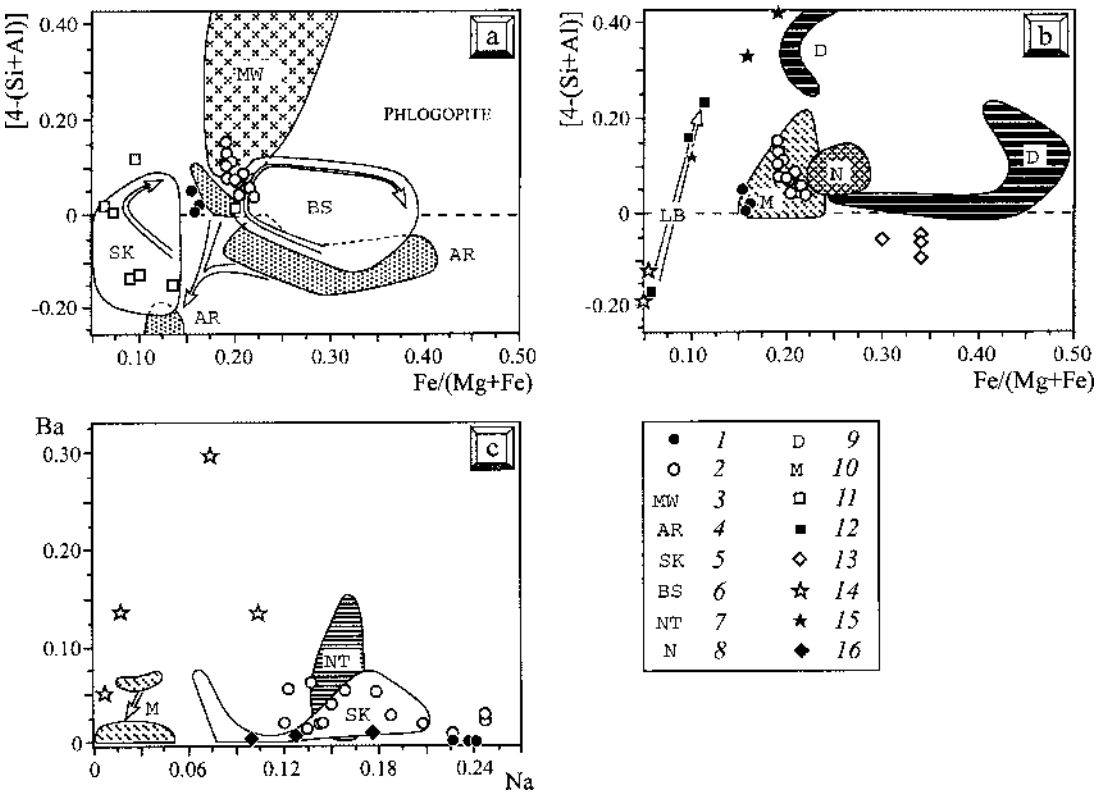

FIG. 4. Compositional variation of phlogopite from Afrikanda (1 ultramafic rocks, 2 CAPR), and other carbonatite complexes, including Mt. Weld in Australia (3), Arkansas (4), Sukulu, Busumbu and Nooitgedacht in Africa (5–7), Newania (8), Dubrava and Murun in Russia (9–10), Fen (11), Loch Borralan (12), Uyaynah in the United Arab Emirates (13), Jacupiranga and Tapira in Brazil (14–15), Blackburn in Canada (16), and Sarfartôq in Greenland. The diagram was constructed using the data of Mitchell (1980), Secher & Larsen (1980), Gaspar & Wyllie (1982), Viladkar & Wimmenauer (1986), Heathcote & McCormick (1989), Hogarth *et al.* (1988), Ouzegane *et al.* (1988), Skosyreva *et al.* (1988), Andersen (1989), Middlemost (1990), Egorov (1991), Woolley *et al.* (1991), Bagdasarov (1994), Young *et al.* (1994), Brigatti *et al.* (1996), McCormick & Le Bas (1996), and Reguir (2001).

contents, and should be classified as magnesiokatophorite (Table 2, anal. 5). The amount of Mn is fairly low in all types of amphibole, slightly decreasing from 0.2–0.4 wt.% MnO in the magnesiohastingsite to <0.2 wt.% MnO in the sodic–calcic varieties; none of the samples contain detectable F. Thus, the overall evolutionary trend exhibited by the amphiboles from CAPR is nearly continuous and involves an increase in Na, Mg, Si and Ti contents, and decrease in the proportions of K, Ca, Fe, Al, Mn and Ti. Note that the compositional variation within the oscillatory-zoned magnesiohastingsite parallels this trend (Fig. 5). In the Afrikanda amphiboles (especially in the late-stage sodic–calcic varieties), the amount of Si and Al is commonly insufficient to fill the tetrahedral sites (Table 2). We arbitrarily ascribed this deficit to the substitution of Fe^{3+} in these sites, as proposed by Hogarth *et al*. (1987) for Ti-poor alkali amphiboles from carbonatite-related fenites. However, Ti^{4+} also may be a viable substituent for Si in richterite (Oberti *et al.* 1992).

Amphiboles are common throughout various carbonatite facies (Samoylov & Gormasheva 1975), and also occur in metasomatized wallrocks (Morbidelli *et al.* 1986). Samoylov (1977) and, subsequently, Hogarth (1989) provided comprehensive reviews of the compositions and mechanisms of substitution operating in amphibole-group minerals from carbonatites. In principle, the evolutionary trend exhibited by the Afrikanda amphiboles mimics that delineated by Samoylov (1977), *i.e.*, Al–Ti-enriched magnesiohastingsite → magnesiokatophorite → richterite → magnesio-arfvedsonite (Fig. 5). Xenocrystic amphiboles and those associated with fenitized ultramafic rocks are commonly pargasitic in composition, being enriched in Al and Ti ± K (Morbidelli *et al.* 1986, McCormick & Heathcote 1987, Young *et al*. 1994). The zoning exhibited by individual crystals from CAPR may be characterized as inverse (increasing Mg and Na contents), using the systematics of zoning patterns developed by Rock *et al*. (1994). Sodic–calcic amphiboles from other carbonatite localities (*e.g.*, Secher & Larsen 1980, Hogarth 1989) may exhibit normal zoning, *i.e*., decreasing Mg coupled with increasing Na contents (in some cases, combined with variations in the proportion of K and other elements). This trend is inferred to result from an increase in $f(O_2)$ during crystallization (Hogarth 1989). A reverse trend, involving an increase in Fe and Ca contents at the expense of Mg and alkalis, has been noted in crystals of

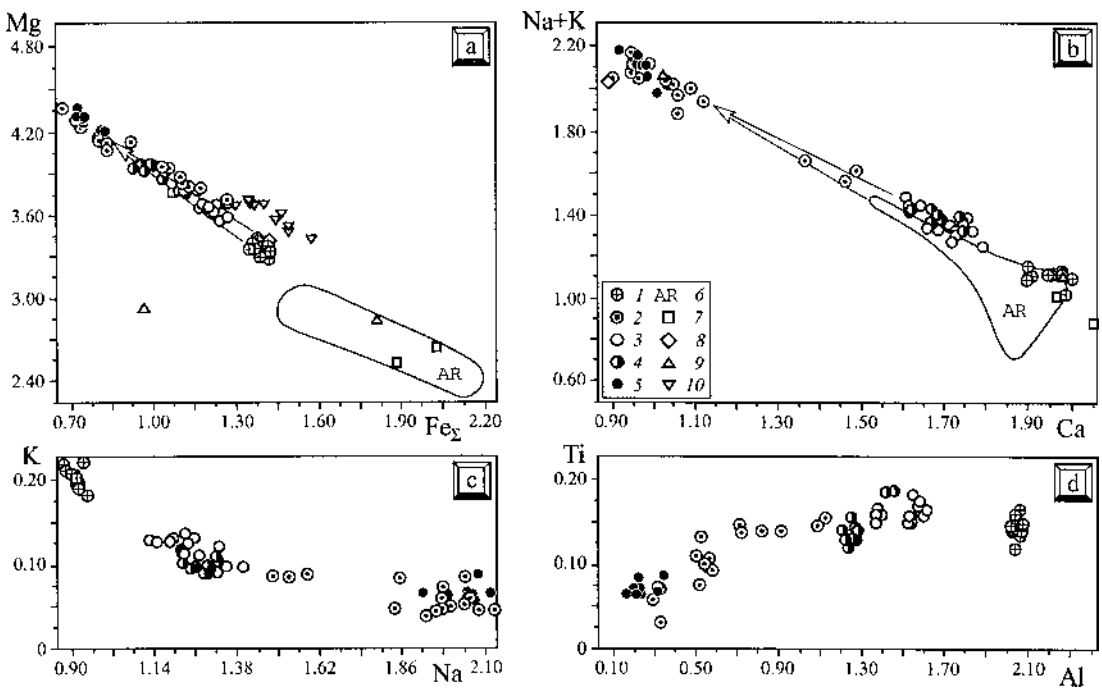

FIG. 5. Variation of major components (*apfu*) in the composition of amphibole-group minerals from CAPR: large crystals of magnesiohastingsite (1), magnesiokatophorite and richterite replacing magnesiohastingsite (2), high-AZ (3), low-AZ (4) zones and richterite rims (5) in oscillatory-zoned crystals. The compositions of amphiboles from the carbonatites of Arkansas (6), In'Ouzzal (7), Fen (8), Turiy Mys (9) and Newania (10) are plotted for comparison (Samoylov 1977, Viladkar & Wimmenauer 1986, McCormick & Heathcote 1987, Ouzegane *et al.* 1988, Andersen 1989).

magnesio-arfvedsonite – richterite from the Rainville mine in Quebec (Hogarth *et al.* 1987) and magnesioriebeckite–winchite from the Mud Tank complex in Australia (Currie *et al*. 1992). Reducing conditions of crystallization (Hogarth 1989) and a late-stage metasomatic overprint (Currie *et al*. 1992) have been invoked to explain the reverse zoning in these cases.

Late-stage parageneses

In CAPR, *titanite* is ubiquitous throughout modally distinct units; its relative proportion increases to 10–15 vol.% in proximity of perovskite or ilmenite segregations. Three macroscopic varieties of titanite were recognized: (i) honey-yellow granular masses replacing the early perovskite (Fig. 1b), interstitial with respect to diopside and magnesiohastingsite, and grading into euhedral wedge- shaped crystals toward the pockets of calcite, (ii) dark brown platy crystals associated with chlorite, and (iii) lemon-yellow masses typically found in an assemblage with ilmenite and zircon. All varieties of titanite deviate significantly from the ideal formula owing to incorporation of other elements in the Ca and Ti sites (Table 3). The honey-yellow crystals are enriched in Fe, Nb and Na; the brown variety contains elevated levels of Al, Nb, Zr and, especially, Fe (0.09–0.10 *apfu*). Titanite (iii) is unique in having a remarkable proportion of Zr while being relatively poor in Nb and Fe. The Zr content varies significantly within the grains (0.03–0.12 *apfu*, or 2.0–7.6 wt.% ZrO_2) and, to our knowledge, is unparalleled by titanite from any other locality. The highest Zr contents previously reported for this mineral are 4.2 wt.% ZrO_2 (Dawson *et al.* 1995), 2.4 wt.% ZrO_2 (Giannetti & Luhr 1983) and 1.9 wt.% ZrO_2 (Della Ventura *et al*. 1999), all from alkaline syenitic rocks. A noteworthy compositional feature of all Afrikanda titanite is its generally low *LREE* contents (*LREE*: light rare-earth elements), significantly

TABLE 3. REPRESENTATIVE COMPOSITIONS AND UNIT-CELL PARAMETERS OF TITANITE

Wt.%	1	2	3	4	5	6	7	8	9	10
Na_2O	0.13	0.34	0.26	0.09	0.04	0.26	0.39	0.34	0.24	0.25
CaO	27.45	27.41	27.35	27.66	27.94	27.75	27.40	27.77	27.65	27.63
Ce_2O_3	0.80	0.66	0.63	0.33	0.40	0.50	0.31	0.34	0.58	0.30
TiO_2	38.64	38.59	38.68	34.15	33.71	38.28	38.59	37.65	36.27	34.90
ZrO_2	0.40	0.13	n.d	0.90	1.25	2.00	2.83	3.71	5.60	7.60
Nb_2O_5	0.79	0.83	0.96	0.90	1.52	0.24	0.06	0.39	0.12	n.d
Fe_2O_3	1.44	1.07	0.82	3.51	4.02	0.78	0.20	0.77	0.14	0.10
Al_2O_3	0.22	0.09	0.08	0.41	0.24	n.d	n.d	n.d	n.d	n.d
SiO_2	29.70	29.93	29.92	30.11	29.20	29.97	30.27	30.26	30.00	29.96
Total	99.57	99.05	98.70	98.06	98.32	99.78	100.05	101.23	100.60	100.74
Structural formulae calculated on the basis of 3 cations:										
Na	0.008	0.022	0.017	0.006	0.003	0.017	0.025	0.022	0.015	0.016
Ca	0.974	0.973	0.975	0.991	1.005	0.982	0.967	0.974	0.982	0.984
Ce	0.010	0.008	0.008	0.004	0.005	0.006	0.004	0.004	0.007	0.004
Σ	0.992	1.003	1.000	1.001	1.013	1.005	0.996	1.000	1.004	1.004
Ti	0.962	0.961	0.967	0.859	0.851	0.950	0.956	0.926	0.904	0.873
Zr	0.006	0.002	-	0.015	0.020	0.032	0.045	0.059	0.091	0.123
Nb	0.012	0.012	0.014	0.014	0.023	0.004	0.001	0.006	0.002	-
Fe*	0.036	0.027	0.021	0.088	0.102	0.019	0.005	0.019	0.003	0.003
Al_{VI}	-	-	-	0.016	-	-	-	-	-	-
Σ	1.016	1.002	1.002	0.992	0.996	1.005	1.007	1.010	1.005	0.999
Al_{IV}	0.009	0.004	0.003	-	0.010	-	-	-	-	-
Si	0.983	0.991	0.995	1.007	0.981	0.990	0.997	0.990	0.996	0.997
Σ	0.992	0.995	0.998	1.007	0.991	0.990	0.997	0.990	0.996	0.997
Unit-cell parameters:										
a, Å	7.0661(6)			7.079(1)				7.074(2)		
b, Å	8.702(1)			8.709(2)				8.707(1)		
c, Å	6.5567(5)			6.5625(6)				6.5599(7)		
β, °	113.837(9)			113.91(1)				113.89(1)		

Compositions: 1-3 honey-yellow wedge-like crystals; 4-5 dark brown platy crystals; 6-10 lemon-yellow anhedral variety. All data this work. Total Fe expressed as Fe_2O_3; n.d = not detected.

below those found in titanite from some alkaline rocks (*e.g.*, Russell *et al.* 1994, Chakhmouradian & Mitchell 1999). Among the lanthanides, only Ce is detectable by EDS; the highest concentrations of this element (0.4–0.8 wt.% Ce_2O_3) are observed in honey-yellow titanite associated with the *LREE*-enriched perovskite.

The unit-cell data for the different varieties of titanite are given in Table 3. Varieties (ii) and (iii) have somewhat longer *a* parameters (along the chains of TiO_6 octahedra) relative to that of pure $CaTiSiO_5$ (*e.g.*, Hughes *et al.* 1997), undoubtedly owing to the larger ionic radii of Fe^{3+}, Nb and Zr in comparison with Ti. All three varieties are inferred to have the *A*2/*a* structure because reflections violating *A*-centering were not observed. Stabilization of the *A*2/*a* structure at room temperature probably results from under- and overbonding of bridging oxygen atoms along the TiO_6 chains because of substitutions in the octahedral site involving Fe^{3+}, Al^{3+} and Nb^{5+} (*cf.* data of Hughes *et al.* 1997).

Zircon is found as scarce crystals embedded in grayish translucent calcite or lemon-yellow titanite; it was never observed in late-stage calcite. Other minerals typically associated with zircon include amphibole, schorlomite and ilmenite. Three morphological types of zircon were distinguished: (i) dark brown grains enclosed in titanite and other silicates, (ii) zoned prismatic crystals (up to 10 mm in length) with a dark brown core similar to type (i) and a pistachio-green rim, and (iii) brownish pink pseudododecahedral crystals up to 1 mm across. The morphology of types (ii) and (iii) is dominated by {100} and {111}, but the ratio between these two forms is different (Fig. 6); {110} is a minor form present in both morphological types. It is noteworthy that bipyramidal zircon is very typical of carbonatites, whereas the crystals of columnar habit are much less common in these rocks (Kukharenko *et al.* 1965, Kozyreva *et al.* 1990).

All three varieties of zircon are metamict, and exhibit characteristic alteration-induced features: optical turbidity, polygonal fracturing in the rim, and sieve-like textures in the interior of crystals, and veining by high-AZ and strongly hydrated low-AZ material (Figs. 7a–c). Compositionally, the Afrikanda zircon is enriched in Th (up to 7.2 wt.% ThO_2). The Hf content is systematically low (<1.4 wt.% HfO_2), and other elements (including U) are present at or below their limits of detection by WDS (Table 4). All morphological types show an essentially identical pattern of chemical zoning involving a decrease in Th and, to a lesser extent, Hf toward the rim. The low-AZ hydrated material developed in fractures contains elevated levels of Ca, and fits the simplified empirical formula $(Zr,Ca)Si(O,OH)_4 \bullet 2.0–2.5H_2O$. The high-AZ material is Th-rich and also contains elevated levels of Ca and *LREE*; some compositions have Th > Zr (*apfu*) and are tentatively identified here as *thorite* (Fig. 7b).

TABLE 4. REPRESENTATIVE COMPOSITIONS OF ZIRCON

Wt.%	1	2	3	4	5	6	7
ZrO_2	59.65	66.26	63.34	65.20	64.41	62.57	64.73
HfO_2	1.16	0.81	1.41	1.02	1.06	1.39	1.03
ThO_2	6.31	0.42	2.22	0.28	0.25	2.72	0.18
UO_2	0.11	0.03	0.07	n.d	n.d	n.d	n.d
CaO	n.d	n.d	0.04	n.d	0.02	n.d	n.d
FeO	0.04	0.05	n.d	n.d	0.02	n.d	n.d
PbO	0.06	n.d	n.d	n.d	0.02	n.d	n.d
Al_2O_3	0.02	0.02	0.03	0.01	0.01	0.02	n.d
SiO_2	30.48	32.27	31.78	32.40	32.40	31.87	32.24
Total	97.83	99.86	98.89	98.91	98.19	98.57	98.18
Structural formulae calculated on the basis of 4 atoms of oxygen:							
Zr	0.947	0.995	0.971	0.985	0.979	0.962	0.984
Hf	0.011	0.007	0.013	0.009	0.009	0.013	0.009
Th	0.047	0.003	0.016	0.002	0.002	0.020	0.001
U	0.001	-	-	-	-	-	-
Ca	-	-	0.001	-	0.001	-	-
Fe	0.001	0.001	-	-	0.001	-	-
Pb	0.001	-	-	-	-	-	-
Σ	1.008	1.006	1.001	0.996	0.991	0.995	0.994
Al	0.001	0.001	0.001	-	-	0.001	-
Si	0.993	0.994	0.999	1.004	1.009	1.005	1.005
Σ	0.994	0.995	1.000	1.004	1.009	1.006	1.005
Hf/Zr	0.012	0.007	0.013	0.009	0.009	0.014	0.009

Compositions: Core (1) and rim (2) of a brown prismatic crystal; (3) brown core, and yellowish green rim (4-5) of a zoned prismatic crystal (Figs. 7 a,b); (6) core and (7) rim of a brownish pink bipyramidal crystal (Fig. 7c). All data this work. Total Fe expressed as FeO; n.d = not detected; n.a = not analyzed.

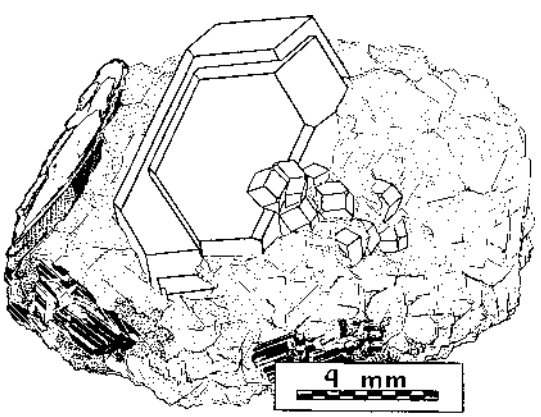

FIG. 6. Schematic drawing showing relationships between the zoned prismatic and brownish pink pseudododecahedral varieties of zircon from CAPR. Both varieties are embedded in calcite (stippled) and associated with platy ilmenite (left), amphibole (black, prismatic) and Zr-enriched titanite (densely stippled).

Although zircon is not uncommon in carbonatites, there is a paucity of reliable compositional data on this mineral. In agreement with our findings, the published analytical results (Heaman *et al.* 1990, Kozyreva *et al.* 1990) show generally low levels of Hf (<1.7 wt.% HfO_2). For the Kola carbonatites, late generations of zircon were observed to have lower Hf/Zr values relative to the earlier-formed generations (Kozyreva *et al.* 1990), in accord with the zoning pattern observed in the crystals from Afrikanda (Table 4). Although low Th/U values have been considered one of the characteristic geochemical signatures of zircon from carbonatites (Group II of Heaman *et al.* 1990), the high Th contents coupled with very low U levels in zircon from CAPR and Kovdor (Amelin & Zaitsev 2002) show that this is not necessarily the case. Clearly, a comprehensive study of material from different localities is required to determine the true compositional range of zircon from carbonatites.

Gittinsite ($CaZrSi_2O_7$) is relatively common at Afrikanda, but does not attain grain sizes larger than 0.1 mm. The identification of this mineral was confirmed by electron-microprobe and optical examination (Table 5). Gittinsite forms anhedral to subhedral crystals associated with schorlomite, titanite and chlorite, or intergrowths with other Zr silicates. Some grains of gittinsite embedded in calcite contain relict fragments of zircon and, in turn, are overgrown by a "corona" of *calcium catapleiite*, $CaZrSi_3O_9 \cdot 2H_2O$ (Fig. 7d). Very few compositions correspond to its Na-analogue, *catapleiite* (Table 5). Gittinsite and catapleiite-group minerals are extremely rare, and generally occur in peralkaline silicate rocks. Gittinsite has been observed in peralkaline granites and syenites of Prince of Wales Island in Alaska and Pajarito in New Mexico (A.N. Mariano, pers. commun.), Kipawa and Strange Lake complexes in eastern Canada (Ansell *et al.* 1980, Birkett *et al.* 1992), and Khaldzan – Buregtey pluton in Mongolia (Kovalenko *et al.* 1995). Afrikanda is the first example of gittinsite occurring in carbonatitic assemblages. Calcium catapleiite and catapleiite are comparatively more common (*e.g.*, Chakhmouradian & Mitchell 2002), but only the latter mineral has been previously encountered in carbonatites, including Kovdor, Vuorijarvi and Sallanlatvi in northwestern Russia (Kapustin 1971, Voloshin *et al.* 1989, Zaitsev *et al.* 1999). The Ca–Zr silicates from Afrikanda contain relatively minor amounts of substituent elements (primarily, Fe, Nb and Ti).

Cerite-(Ce), confirmed by XRD [*a* 10.77(1), *c* 38.06(6) Å], is a characteristic accessory phase invariably associated with the primary calcite. Other minerals commonly found in the same assemblage include titanite, loparite-(Ce), ancylite-group and chlorite-group minerals and goethite. Crystals of cerite-(Ce) are typically arranged in clusters. Clusters embedded in calcite consist of randomly oriented elongate crystals up to 50 μm in length, typically showing a relatively low-AZ rim up to a few μm in thickness (Fig. 8a). Cerite-(Ce) enclosed in chlorite forms groups of nearly equant rhom-

TABLE 5. REPRESENTATIVE COMPOSITIONS OF Ca-Zr SILICATES

Wt.%	1	2	3		1	2	3
				Structural formulae calculated on the basis of:			
					O = 7	O = 9	
Na_2O	n.d	5.40	3.15	Na	-	0.671	0.396
CaO	17.91	9.43	9.52	Ca	0.977	0.647	0.661
MgO	n.d	0.17	0.16	Mg	-	0.016	0.015
FeO	0.47	0.27	0.24	Fe	0.020	0.014	0.013
				Σ	0.997	1.348	1.085
Al_2O_3	0.20	n.d	n.d	Al	0.012	-	-
ZrO_2	38.74	31.29	31.02	Zr	0.962	0.977	0.980
TiO_2	0.05	0.15	0.22	Ti	0.002	0.007	0.011
HfO_2	0.84	n.d	n.d	Hf	0.012	-	-
Nb_2O_5	0.15	0.46	0.59	Nb	0.003	0.013	0.017
				Σ	0.991	0.997	1.008
SiO_2	39.50	46.72	47.01	Si	2.012	2.992	3.045
Total	97.86	93.89	91.91				

Compositions: 1 gittinsite; 2 catapleiite; 3 calcium catapleiite (Fig. 7d). All data this work. Total Fe expressed as FeO; n.d = not detected; n.a = not analyzed.

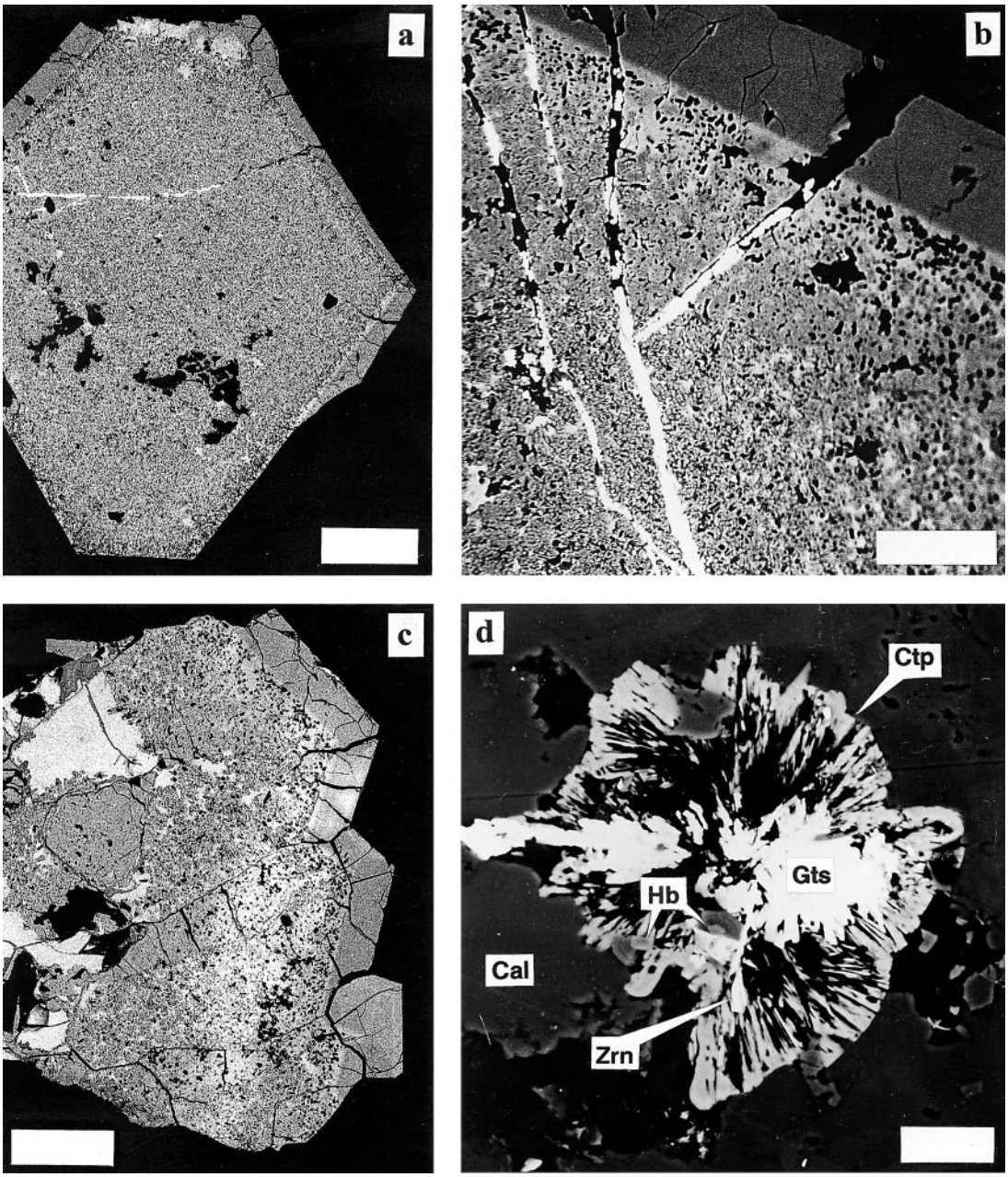

FIG. 7. BSE images showing the pattern of zoning in zircon crystals from CAPR and textural relationships among different Zr minerals in CAPR. (a) Prismatic crystal with a Th-rich core and comparatively Th–Hf-depleted rim, scale bar 200 μm; (b) detail of (a) showing the "spongy" texture of Th-rich zircon and fractures filled with thorite (white), scale bar 50 μm; (c) cluster of pseudododecahedral crystals of zircon with a Th–Hf-depleted rim, scale bar 200 μm; (d) gittinsite (Gts) overgrown by calcium catapleiite and catapleiite (Ctp); note the relics of zircon (Zrn) and fragments of hibschite (Hb) in the zirconosilicates, scale bar 30 μm.

bohedra ranging from 5 to 50 μm across. Some of these crystals contain cubic inclusions of thorianite and loparite-(Ce). The greatest morphological diversity is exhibited by cerite-(Ce) confined to calcite-filled fractures and pockets in perovskite (Figs. 8b–f). Along some of the fractures, perovskite is mantled successively by loparite-(Ce) (up to 10 μm in thickness), titanite (5–20 μm) and cerite-(Ce) (<5 μm). More-or-less equant clusters of cerite-(Ce) "perched" on titanite appear to be intergrowths of numerous flattened rhombohedral crystals of varying size (Fig. 8b). BSE imaging reveals the intricacy and compositional heterogeneity of such intergrowths (Figs. 8d–f). Individual crystals display an oscillatory pattern of zoning, with comparatively lower-AZ zones commonly having an altered, "boxwork" or "spongy" appearance. Some crystals are partially replaced by calcio-ancylite-(Ce). The order of crystallization deduced from textural relationships (*e.g.*, Fig. 8c) is invariably perovskite → loparite-(Ce) → titanite → cerite-(Ce) → goethite → calcite and ancylite-group minerals. In thin section, cerite-(Ce) is pleochroic from colorless to clove-pink, uniaxial positive, has high indi-

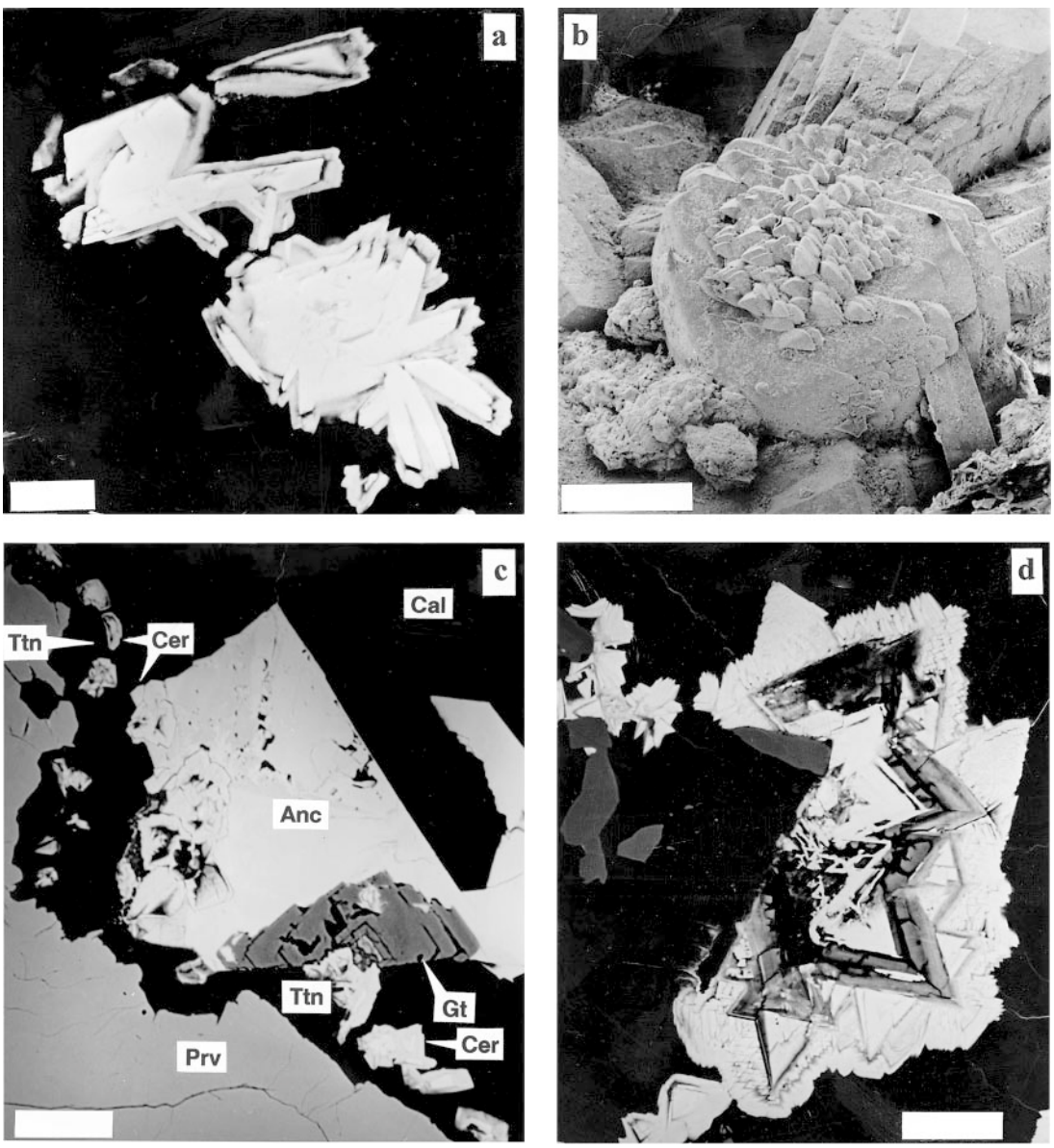

ces of refraction (>1.800), and a low birefringence (0.004).

The analysis of cerite-(Ce) from CAPR is difficult owing to the complexity of zoning, high H_2O contents in the low-AZ zones, and intimate association of this mineral with ancylite-(Ce). Another complication is the paucity of compositional data for cerite-(Ce) from other localities, *i.e.*, a lack of suitable references. This mineral has been previously described from diverse petrographic settings, including carbonatites (Glass *et al.* 1958, Moecher *et al.* 1997), fenites (Kapustin 1989), peralkaline nepheline syenite pegmatites (Horváth & Gault 1990), granites and granitic pegmatites (Sabina 1964, Förster 2000), and hence, shows a significant variation in chemistry. Moore & Shen (1983) determined the close structural similarity between cerite-(Ce) and whitlockite, and proposed for the former mineral the following structural formula: $(LREE,Ca)_9(Fe^{3+},Mg,Al)(SiO_4)_6(SiO_3OH)(OH)_3$. However, most of the analyses available in the literature deviate from this formula toward lower Si contents. If we use for comparative purposes the most recent and reliable data, the amount of Si in cerite-(Ce) ranges from 6.11 (Ulan-Erge, Tuva) to 6.83 *apfu* (Erzgebirge, Germany) (Kapustin 1989, Förster 2000). The Afrikanda material is unlike any of the previously described examples, as it contains a large proportion of Ca relative to *LREE* (5.9–9.3 wt.% CaO; Ca/*LREE* in the range 0.28–0.46), combined with high Fe contents (up to 3.9 wt.% Fe_2O_3) and a lack of detectable Mg (Table 6). A high proportion of Ca was observed in cerite-(La) by Pakhomovsky *et al.* (2002); they proposed that Ca in this mineral enters not only the *REE* positions, but also the Fe^{3+}-dominant site and a low-occupancy Ca site. This interpretation is consistent with (*REE* + Ca) > 9 *apfu* in the composition of Afrikanda material. Pakhomovsky *et al.* (2002) also modified the general formula of cerite-type minerals as $REE_9(Fe,Mg,Ca)Ca_x[SiO_4]_3[SiO_3(OH)_{1-x}O_x]_3[SiO_3(OH)]_{1-x}(OH)_3$. Our data recalculated to a total of 17 cations, give a nearly stoichiometric amount of Si for the high-AZ areas, and a systematically lower number of Si atoms for the low-AZ areas (Table 6, anal. 4). This deficiency of cations in the tetrahedral sites may result from partial substitution of Si by hydroxyl groups (as in "hydrogarnets"). An alternative substitution involving complex anions $(FCO_3)^{3-}$ was suggested by Glass *et al.* (1958), but was not confirmed by the structural work of Moore & Shen (1983).

Chlorite-group minerals are ubiquitous in CAPR, and occur as fracture fillings in amphibole (Figs. 1b, d), and also as spherulites, sheaves and books of bent pseudohexagonal crystals (Fig. 9). In both calcite-rich and primarily diopside–magnesiohastingsite parageneses, the chlorite is confined to cavities, interstices and fractures in the earlier-crystallized phases. The mineral ranges from silvery to olive green in color, reflecting the compositional variation from clinochlore to chamosite [0.25 < Fe/(Fe + Mg) < 0.71]. The spherulites typically contain a core of intermediate Fe/(Fe + Mg) value (0.53–0.56), three or four transitional zones composed of alternating chamosite and clinochlore, and a rim that may be Mg- or Fe-rich (Fig. 9a, Table 7, anal.

FIG. 8. BSE images (a, c–f) and SEM image (b) showing the occurrence of cerite-(Ce) in CAPR and its relationships with other minerals: Prv: perovskite, Ttn: titanite, Cer: cerite-(Ce), Gt: goethite, Anc: ancylite-(Ce) zoned toward calcio-ancylite-(Ce), Cal: calcite. Scale bars: 15 μm (a), 100 μm (b), 50 μm (c, e), 30 μm (d), and 40 μm (f).

1–4). The late generation of chlorite making up the rim is poorer in Mn and Ti in comparison with the earlier-crystallized generations comprising the bulk of the spherulites and replacing the amphibole (Table 7, anal. 5). On the $Fe\Sigma/(Fe + Mg)$ *versus* Si diagram (Fig. 10), the compositions of Afrikanda chlorite delineate a trend that, however, is not a true evolutionary trend, because the patterns of zoning in individual spherulites involve both increases and decreases in Fe/(Fe + Mg), and, in general, are poorly correlated. Limited data available on chlorite from other carbonatite occurrences show that it is quite variable in composition (Fig. 10).

TABLE 6. REPRESENTATIVE COMPOSITIONS OF CERITE-(Ce)

Wt.%	1	2	3	4	5	6
CaO	6.38	6.69	6.81	6.35	8.89	9.33
SrO	n.d	n.d	n.d	0.10	n.d	n.d
La_2O_3	11.31	9.45	6.46	9.50	12.08	12.02
Ce_2O_3	34.19	33.74	31.89	27.45	28.60	28.85
Pr_2O_3	3.74	4.11	3.85	4.19	5.66	6.28
Nd_2O_3	14.27	15.94	20.01	10.33	12.71	11.64
Sm_2O_3	0.90	1.11	0.76	0.49	0.59	0.16
Gd_2O_3	0.27	0.33	1.49	n.d	0.43	0.75
ThO_2	0.04	n.d	n.d	1.21	0.46	0.26
Al_2O_3	0.78	0.48	0.39	0.81	0.78	0.60
Fe_2O_3	1.21	1.42	1.91	3.03	2.95	2.71
SiO_2	22.56	22.32	22.31	18.86	24.22	24.18
P_2O_5	0.25	n.d	0.08	n.d	n.d	n.d
Total	95.90	95.59	95.96	82.32	97.37	96.78
Structural formulae calculated on the basis of 17 cations						
Ca	2.113	2.230	2.258	2.401	2.751	2.894
Sr	-	-	-	0.020	-	-
La	1.290	1.084	0.737	1.237	1.287	1.283
Ce	3.870	3.843	3.614	3.547	3.024	3.058
Pr	0.421	0.466	0.434	0.539	0.596	0.662
Nd	1.576	1.772	2.212	1.302	1.311	1.204
Sm	0.096	0.119	0.081	0.060	0.059	0.016
Gd	0.028	0.034	0.153	-	0.041	0.072
Th	0.003	-	-	0.097	0.030	0.017
Σ	9.397	9.548	9.489	9.203	9.099	9.206
Al	0.284	0.176	0.142	0.337	0.266	0.205
Fe*	0.281	0.332	0.445	0.805	0.641	0.590
Σ	0.565	0.508	0.587	1.142	0.907	0.795
Si	6.973	6.944	6.903	6.655	6.994	6.999
P	0.065	-	0.021	-	-	-
Σ	7.038	6.944	6.924	6.655	6.994	6.999

Compositions: 1-3 elongate crystals in a calcite matrix (Fig. 8a); 4-6 cluster of crystals (Figs. 8 b-f): low-AZ core (4) intergrown with calcio-ancylite-(Ce), and high-AZ rim (5-6). All data this work. Total Fe expressed as Fe_2O_3; n.d = not detected.

A silicate of Ca and Al provisionally identified in this work as *cebollite* is relatively uncommon in CAPR; it occurs exclusively in a paragenesis with titanite, hibschite and chlorite. Cebollite crystallized nearly simultaneously with titanite in proximity to the discrete laths of ilmenite, and commonly in fractures within these laths (Fig. 11a). The mineral forms concentrically zoned spherulites ranging from 30 to 120 μm in diameter, and consisting of colorless radiating fibers. Some spherulites contain fragments of ilmenite and, in turn, may be enclosed by titanite; both cebollite and titanite crystallize prior to the spherulitic chlorite. The composition of the Afrikanda cebollite is best recalculated to a total of 10 cations (Table 7, anal. 6–7); this approach yields formulae with 3 *apfu* Si, *i.e.*, similar to that proposed in the original study by Larsen & Schaller (1914). All spherulites have an oscillatory-type pattern of zoning in BSE, arising from variations in the proportion of Ti. Cebollite is a poorly characterized mineral whose actual chemical composition and crystal structure have not been determined to date. A detailed study of the Afrikanda material is currently under way.

Euhedral crystals of *hibschite* some 10–30 μm across occur in fractures within the primary calcite, in parts of the rock enriched in chlorite, cebollite and other late-stage Ca silicates (Fig. 11b). We did not observe hibschite in association with schorlomite, although such an assemblage is not impossible, taking into consideration the common occurrence of "hydrogrossular" as a mantle on Ti-bearing garnets from diverse alkaline rocks (*e.g.*, Flohr & Ross 1989, Ulrych *et al.* 1994). In thin section, the crystals of hibschite are colorless, isotropic, and exhibit oscillatory zoning arising from changes in index of refraction. This zoning appears to be related to variations in the Fe:Al ratio (Fig. 11b); the proportions of Ca, Mn and Ti remain nearly constant across the crystal (Table 7, anal. 8–10). The composition of the low-AZ zones approaches the ideal formula, whereas the high-AZ areas contain up to 20 mol.% of the Fe-dominant "end-member", $Ca_3Fe_2(SiO_4)_{3-x}(OH)_{4x}$. The ferric-iron-dominant analogue of hibschite has been described from metamorphic rocks of San Benito in California, and the Wessels mine in South Africa (Lager *et al.* 1989, Armbruster 1995), but has not been submitted to IMA for approval (J.A. Mandarino, pers. commun.).

Zeolites occur interstitially with respect to calcite, and locally form compact masses of pale pink color composed largely of natrolite [confirmed by XRD: *a* 18.255(9), *b* 18.60(1), *c* 6.62(1) Å]. Flakes of muscovite, interstitial grains and tetragonal crystals of edingtonite (confirmed by XRD), and "lamellae" of an unidentified Na–Ca–Sr zeolite are present in lesser amounts, invariably in association with natrolite. Natrolite, edingtonite (Table 8, anal. 1) and muscovite are close to their ideal compositions, whereas the Na–Ca–Sr phase shows a significant variation in Sr content that correlates antipathetically with the proportion of Ca (Table 8, anal. 2–4). In terms of stoichiometry, this min-

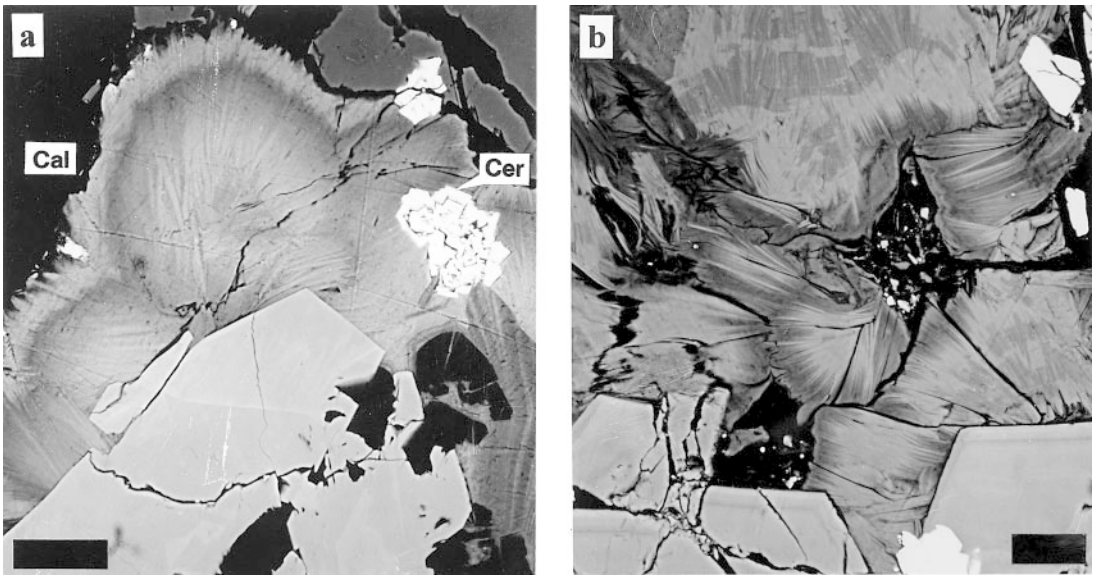

FIG. 9. BSE images showing chlorite spherulites composed of chamosite (lighter bands) and clinochlore (darker bands) associated with ilmenite and perovskite (light gray), cerite-(Ce) (Cer) and calcite (Cal). Scale bars are 50 μm (a) and 30 μm (b).

eral approaches the empirical formula $Na_2(Ca_{1.5-2.0}Sr_{1.0-1.5})_{\Sigma 3}(Al_8Si_8O_{32})\bullet nH_2O$, and is unlike any of the known Sr-bearing zeolites, but may represent a strontium-rich variety of thomsonite (I.V. Pekov, pers. commun.). Prehnite (Table 8, anal. 5) was found in a single specimen as poikilitic crystals enclosing multiple grains of cerite-(Ce) and calcio-ancylite-(Ce). Previously, Fe-bearing prehnite in association with natrolite, edingtonite and other zeolites had been observed at Afrikanda in hydrothermally altered alkaline pegmatites emplaced after CAPR (Kukharenko *et al.* 1965, Pekov *et al.* 2001).

DISCUSSION

Crystallization history: the magmatic stage

In CAPR, Ti- and Al-poor diopside and magnesiohastingsite were the earliest silicate minerals to crystallize. Schorlomite is present sporadically and only in minor amounts, possibly indicating that its crystallization was controlled by local fluctuations in the activity of silica (Chakhmouradian & Zaitsev 1999). Although CAPR does contain xenocrysts of clinopyroxene, magnetite and perovskite derived from the wallrock ultramafic rocks, there is no textural evidence to suggest that the diopside from CAPR crystallized by metasomatic replacement of the wallrock or at the expense of Ti–Al-rich xenocrystic clinopyroxene. The compositional contrast between the clinopyroxene from CAPR and clinopyroxenites, and the absence of intermediate com-

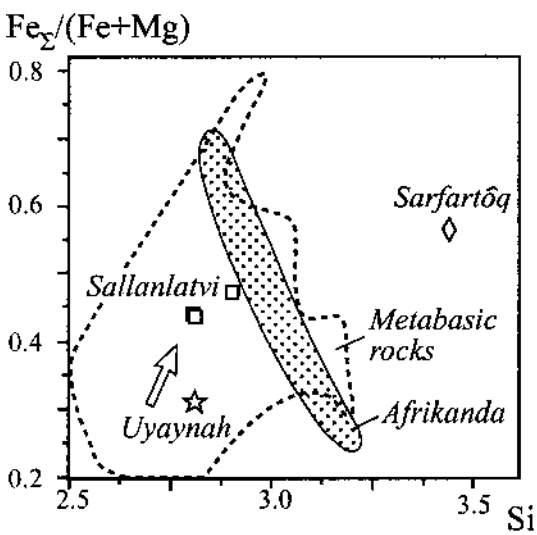

FIG. 10. Composition of chlorite from CAPR and other carbonatite complexes (from Secher & Larsen 1980, Woolley *et al.* 1991, and authors' unpubl. data). The field of chlorite from metabasic rocks and the trend of decreasing metamorphic grade (arrow) are adopted from Zane *et al.* (1998).

TABLE 7. REPRESENTATIVE COMPOSITIONS OF CHLORITE AND LATE-STAGE Ca SILICATES

Wt.%	1*	2*	3*	4*	5*	6†	7†	8†	9†	10†
	C H L O R I T E					CEBOLLITE		HIBSCHITE		
CaO	0.19	0.18	0.15	0.11	0.34	35.38	36.16	37.32	37.25	37.47
MnO	0.74	0.86	0.75	0.02	1.00	0.04	n.d	0.04	0.04	n.d
MgO	13.16	7.70	9.58	20.66	24.45	n.d	n.d	n.d	n.d	n.d
FeO	29.25	33.61	32.10	19.73	15.20					
Fe_2O_3						1.96	2.05	4.69	5.17	2.32
TiO_2	0.09	0.16	0.12	n.d	0.05	9.44	2.69	0.13	n.d	n.d
Al_2O_3	16.75	18.82	17.91	16.79	14.16	14.40	18.60	19.38	18.98	21.04
SiO_2	27.31	25.53	25.26	29.60	32.02	27.13	27.62	27.28	28.06	27.52
Total	87.49	86.86	85.87	86.91	87.22	88.35	87.12	88.84	89.50	88.35
Structural formulae calculated on the basis of:										
			O = 14			Σ cations = 10		Ca + Mn = 3		
Ca	0.022	0.022	0.018	0.012	0.037	4.183	4.218	2.997	2.997	3.000
Mn	0.068	0.082	0.072	0.002	0.085	0.004	-	0.003	0.003	-
Mg	2.125	1.285	1.609	3.164	3.658	-	-	-	-	-
Fe^{2+}	2.649	3.146	3.024	1.695	1.275	-	-	-	-	-
Fe^{3+}	-	-	-	-	-	0.163	0.168	0.265	0.292	0.131
Ti	0.007	0.013	0.010	-	0.004	0.783	0.220	0.007	-	-
Al_{VI}	1.095	1.340	1.223	1.072	0.888	1.873	2.387	1.712	1.680	1.853
Σ	5.966	5.888	5.956	5.945	5.947	7.006	6.993	4.984	4.972	4.984
Al_{IV}	1.043	1.143	1.155	0.960	0.787	-	-	-	-	-
Si	2.957	2.857	2.845	3.040	3.213	2.994	3.007	2.045	2.107	2.056
Σ	4.000	4.000	4.000	4.000	4.000	2.994	3.007	2.045	2.107	2.056

Compositions: 1-5 chlorite: chamosite core (1), intermediate zone (2), clinochlore intermediate zone (3) and chamosite rim (4) of a spherulite; 5 clinochlore replacing amphibole (Fig. 1d); (6) core and (7) rim of a cebollite spherulite (Fig. 11a); 8-10 core, high-AZ intermediate zone and rim of a hibschite crystal (Fig. 11b). All data this work. * Total Fe expressed as FeO; † total Fe expressed as Fe_2O_3; n.d = not detected.

positions (Table 1, Fig. 2) indicate that they are unlikely to be derived from a common source, or interrelated by a simple crystal-fractionation mechanism. The low contents of Al and Ti, and the lack of zoning in the CAPR diopside, attest to slow, equilibrium growth in a relatively low-*P* and low-*T* environment. Clinopyroxene of broadly similar composition is found in many plutonic carbonatites, including the Turiy Mys complex in Kola and the Maimecha–Kotuy group of intrusions in Siberia (Fig. 2). The latter also feature phoscoritic rocks composed of Ti–Al-poor diopside (Egorov 1991, Bagdasarov 1994). Significant variation of the Al and Ti contents observed in some occurrences (*e.g.*, Arkansas) may indicate polybaric crystallization, possibly in combination with rapid rates of cooling (Gamble & Taylor 1980, Kouchi *et al.* 1983; see also a review by Rock *et al.* 1994). The "anomalously" Ti-rich clinopyroxenes studied by Andersen (1988) differ from other examples in containing large proportions of the aegirine component. The Ti enrichment in this mineral may be explained by charge-balance considerations, or simply by the absence of a competitive Ti host (*e.g.*, schorlomite or magnetite) in the Fen carbonatite.

Diopside-rich carbonatites and phoscorites (*e.g.*, Bagdasarov 1994) are less common than forsterite-bearing varieties, and always confined to the early stages of carbonatite genesis. According to the experimental data of Otto & Wyllie (1993), diopside occurs in the subsolidus assemblage of carbonatitic melts with >17 wt.% SiO_2. In the reasonable range of Ca/Mg and H_2O/CO_2 values, precipitation of early phenocrysts of diopside should be expected only from extremely silica-rich

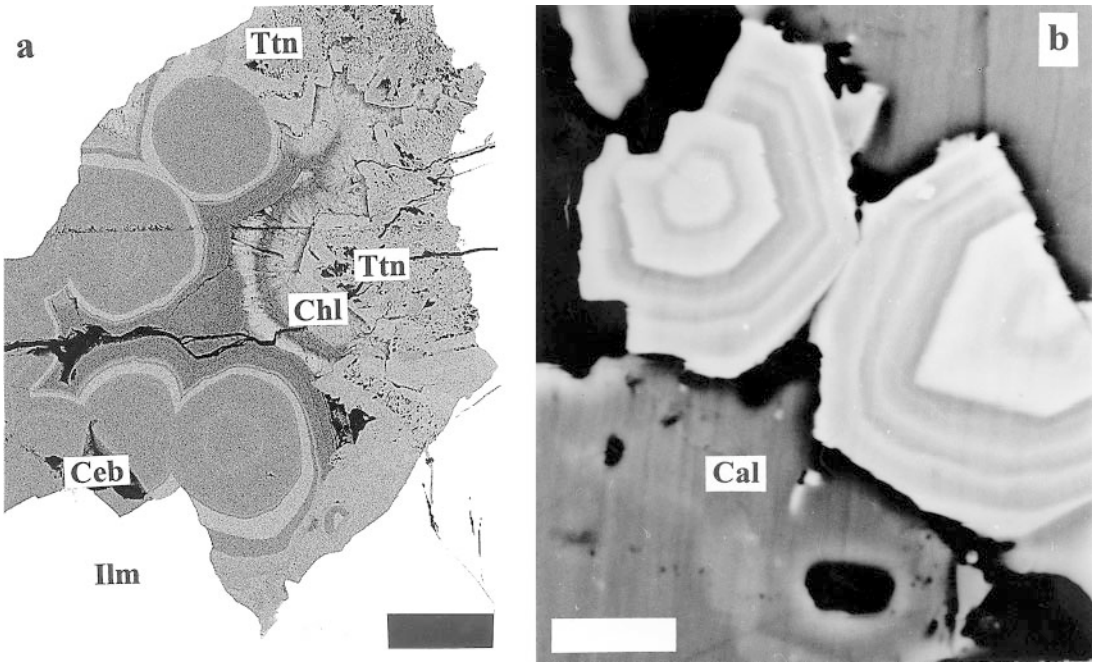

FIG. 11. BSE images showing textural relationships of the late-stage Ca minerals from CAPR. (a) Concentrically zoned spherulites of cebollite (Ceb) and chlorite (Chl) associated with titanite (Ttn) lining a pocket in ilmenite (Ilm), scale bar 60 μm; (b) oscillatory-zoned crystals of hibschite in a fracture within calcite (Cal), scale bar 10 μm.

TABLE 8. REPRESENTATIVE COMPOSITIONS OF ZEOLITES AND PREHNITE

Wt.%	1	2	3	4	5		1	2	3	4	5
	EDINGTONITE	THOMSONITE ?			PREHNITE		EDINGTONITE	THOMSONITE ?			PREHNITE
							Structural formulae calculated on the basis of:				
							(Si+Al) = 7	(Si+Al+Fe) = 16			O = 11
Na_2O	0.42	4.62	3.91	4.49	n.d	Na	0.068	2.124	1.796	2.117	-
K_2O	0.09	0.01	n.d	0.07	n.a	K	0.010	0.003	-	0.021	-
CaO	n.d	5.56	7.74	8.17	27.01	Ca	-	1.413	1.965	2.131	2.010
SrO	n.d	10.57	7.76	6.65	n.a	Sr	-	1.454	1.066	0.938	-
BaO	30.00	0.03	0.06	n.d	n.a	Ba	0.977	0.003	0.006	-	-
						Σ	1.054	4.997	4.833	5.207	2.010
Al_2O_3	20.13	27.44	27.97	27.67	24.08	Al	1.970	7.670	7.811	7.936	1.971
Fe_2O_3	n.d	0.08	0.06	n.d	0.85	Fe	-	0.014	0.011	-	0.045
SiO_2	36.48	35.07	34.52	33.15	42.96	Si	3.030	8.316	8.178	8.064	2.983
						Σ	5.000	16.000	16.000	16.000	7.009
Total	87.12	83.38	82.02	80.20	94.90						
H_2O	12.88	16.62	17.98	19.80		H_2O	3.57	13.16	14.22	16.08	-

Compositions: 1 euhedal edingtonite crystal; 2-4 "lamellae" of an unidentified Na-Ca-Sr zeolite (thomsonite ?) in natrolite; 5 poikilitic prehnite. All data this work. Total Fe expressed as Fe_2O_3; H_2O calculated for the zeolites from the difference of their analysis totals to 100 wt.%. n.d = not detected; n.a = not analyzed.

(≥40 wt.% SiO_2) magmas; Otto & Wyllie interpreted the liquidus field for diopside to lie above 1000°C at 2 kbar. In systems free of alkalis and Al, diopside is accompanied below the solidus by a carbothermal fluid and forsterite. This order of crystallization has been established for phoscorites of the Yraas intrusion, Maimecha–Kotuy (Bagdasarov 1994). Åkermanite ($Ca_2MgSi_2O_7$) may occur in this assemblage at high temperatures and low pressures (generally, <6 kbar), but will be replaced by diopside plus calcite as temperatures decrease, *i.e.*, at 1000°C at 2 kbar in the absence of H_2O (Yoder 1975), and about 950°C at $H_2O/CO_2 >> 0.3$. The instability of åkermanite in the presence of CO_2 explains the scarcity of melilite-bearing carbonatites that occur primarily at the contact of melilitic rocks with carbonatitic intrusions (*e.g.*, Bulakh & Ivanikov 1984, Egorov 1991). In natural systems, the crystallization of olivine will likely be hindered by increasing activities of alkalis and volatiles in a carbonatitic magma, which can ultimately lead to the precipitation of phlogopite or amphibole. In CAPR, the increase in $a(Na^{1+})$ at the early magmatic stage is well documented by the evolution of clinopyroxene compositions from 6 to 17 mol.% *Ae*. Note also that the source of Na could not be extrinsic because the associated ultramafic rocks are cumulate in nature and contain very little alkalis (≤0.5 wt.% $Na_2O + K_2O$ in the olivinites, and ≤1.0 wt.% $Na_2O + K_2O$ in the clinopyroxenites: J. Moutte and D. Garcia, pers. commun.), whereas the foidolites are clearly younger than CAPR.

In many carbonatite complexes, Na and K are effectively removed from the carbonatitic melt through fenitization of the country rocks (Gittins *et al.* 1975, Andersen 1989). The enrichment of fenitizing fluid in Na relative to Ca and Mg has been recently demonstrated experimentally (Veksler & Keppler 2000). At Afrikanda, the extent of alkali metasomatism in the wallrock clinopyroxenites is *very* limited, suggesting that the bulk of Na was retained in the carbonatitic melt, facilitating the crystallization of amphibole. This conclusion is further supported by the occurrence of primary inclusions of Na-bearing carbonates (shortite, burbankite, *etc.*) and lueshite ($NaNbO_3$) in the oxide minerals and hydroxylapatite from CAPR (Zaitsev & Chakhmouradian 2002). From the lack of a fenitization aureole around CAPR and the presence of Na-carbonate inclusions, we infer that the magnesiohastingsite precipitated prior to separation of a fluid from the parental "silicocarbonatite" (see below). The observed textural disequilibrium between the clinopyroxene and amphibole in CAPR (Fig. 1c) possibly indicates a peritectic relationship between these two minerals. Such a conclusion is consistent with the incongruent melting behavior of hastingsitic–pargasitic amphiboles; note also that the products of amphibole breakdown always include clinopyroxene (Gilbert *et al.* 1982).

The inverse zoning of the CAPR amphiboles (increasing proportions of Mg and Na, combined with decreasing Al, K and Ti contents) closely mimics compositional trends exhibited by amphibole-group minerals from some greenschist- and amphibolite-facies metabasic rocks (*e.g.*, Holland & Richardson 1979). Although the algorithm of Holland & Richardson (1979) can be used to calculate the equilibrium *T* and *P* for amphiboles from metamorphic assemblages evolving isochemically, it yields unrealistically high pressures for the CAPR amphiboles because the transition from magnesiohastingsite to magnesiokatophorite to richterite *was not* isochemical. The occurrence of sodic–calcic amphiboles along the rim and cleavage fractures in magnesiohastingsite suggests that they represent products of re-equilibration between the primary calcic amphibole and a Na-rich fluid. Hence, we infer that the onset of crystallization of the sodic–calcic amphiboles in CAPR marks a transition from the early magmatic stage to a hydrothermal stage. Separation of the fluid phase and extensive fracturing were likely induced by decompression of the ascending carbonatitic mush.

Phlogopite appears to be a more common hydrous silicate in carbonatites than calcic amphiboles. At Afrikanda, crystallization of magnesiohastingsite was probably favored by initially high Na/K values of the parental magma. Minor phlogopite is also present here, but its temporal relationships with the amphiboles are not unequivocal. Kukharenko *et al.* (1965) suggested that phlogopite crystallized during the final ("biotite–zeolite") stage of the evolutionary history of CAPR, after the calcic amphibole and the bulk of calcite, but prior to chlorite-group phases. We believe that such an interpretation is inconsistent with the evolutionary trend exhibited by the CAPR amphiboles (in the direction of decreasing K and Al contents), and does not explain the absence of phlogopite in calcite–chlorite-rich zones of the rock. Crystallization of phlogopite probably commenced nearly simultaneously with magnesiohastingsite, but soon ceased because K and Al were depleted from the system. Hence, we suggest that diopside, magnesiohastingsite and phlogopite are primary phases in CAPR, and their occurrence here reflects the enrichment of a parental carbonatitic magma in silica and alkalis. The bulk of this primary paragenesis crystallized in a temperature range between the liquidus field of diopside (*i.e.*, close to 1000°C estimated for alkali-free compositions by Otto & Wyllie 1993) and about 600°C (*i.e.*, above the temperature of inception of exsolution in magnetite–ilmenite: Chakhmouradian & Zaitsev 1999). The latter value is in agreement with the equilibrium crystallization of calcite and nyerereite from blebs of carbonatitic melt entrapped in the magnetite (Zaitsev & Chakhmouradian 2002).

Postmagmatic processes

Although minor in volume, the late-stage association of minerals in CAPR is undoubtedly the most interesting from a mineralogist's standpoint. About forty

out of fifty-six minerals identified in this rock are genetically associated with postmagmatic processes involving primarily precipitation from low-*T* hydrothermal fluids and re-equilibration of the earlier-crystallized phases with these fluids. The major products of re-equilibration are sodic–calcic amphiboles, ceroan perovskite transitional to loparite-(Ce) and ceroan lueshite, titanite and andradite. The fluid fractionated from the carbonatitic parent was initially enriched in Na, *LREE*, Nb and Th, and had a silica activity sufficient for the conversion of perovskite to titanite (Appendix, reaction 1), *i.e.* above 10^{-5} at 300°C, or 10^{-6} at 200°C. The reaction between ilmenite and the fluid to produce titanite (Appendix, reaction 2) is virtually independent of temperature above 150°C, and requires silica activities in excess of 10^{-4}. The onset of titanite crystallization may indicate a gradual decrease in temperature at a constant activity of silica or, less likely, an increase in silica activity due to assimilation of the wallrock material.

The ubiquitous replacement of the amphiboles by chlorite at the final states of evolution indicates an increasingly acidic character of the fluid (Appendix, reaction 3). This conclusion is supported by the occurrence of ancylite-group minerals in CAPR (Zaitsev & Chakhmouradian 2002), as the available experimental data (*e.g.*, Tareen *et al.* 1980) indicate that these phases are unstable in alkaline solutions. In our case, the lower limit of $-\log a(H^+)$ and $\log f(CO_2)$ is defined by dissociation of calcite (Appendix, reaction 4), whereas the upper limit of $\log f(CO_2)$ is constrained by the equilibrium of titanite with anatase plus calcite (Appendix, reaction 5). The equilibrium conditions for all five reactions were assessed for different temperatures at $a(H_4SiO_4)^0 = 10^{-4}$, assuming "ideal" compositions of the minerals involved (Fig. 12). The value of $a(Al^{3+})$ was arbitrarily set at 10^{-6}; an increase in $a(Al^{3+})$ will only slightly affect the amphibole–chlorite equilibrium, shifting it to higher values of $-\log a(H^+)$. A decrease in the activity of silica would have a similar effect, but it is unlikely that $a(H_4SiO_4)^0$ was much lower than 10^{-4}. From Figure 12, it is clear that the three phases making up the bulk of the late-stage paragenesis (*i.e.*, calcite, chlorite and titanite) stably coexist in a relatively limited range of $\log a(H^+)$ and $\log f(CO_2)$. At 300°C, their stability field is near $\log a(H^+) = -4$ and $\log f(CO_2) = 1$, but shifts to lower values as temperature decreases (Fig. 12). This observation implies that the acidity of the fluid, or the partial pressure of CO_2, did not have to change to induce chloritization of the amphibole. On the contrary, CAPR could (and, most likely, did) evolve as a closed system under gradually decreasing temperature. A rough estimate of temperature for reaction (3) may be obtained using the geothermometers for hydrothermal chlorite (Kranidiotis & MacLean 1987, Cathelineau 1988). Assuming that the clinochlore replacing the magnesiohastingsite (Fig. 1d; Table 7, anal. 5) was in equilibrium with the carbothermal fluid, both of the above geothermometers yield values near 190–200°C. Although the late-stage spherulitic chlorite has higher Fe/(Fe + Mg) values than the clinochlore developed after the amphibole, this trend is unlikely to reflect a significant drop in temperature, as suggested by Zane *et al.* (1998) for chlorites from metabasic rocks (arrow in Fig. 10). According to Hillier & Velde (1991), the proportion of octahedrally coordinated cations in chlorite is controlled primarily by compositional parameters in the environment of the crystallization; this conclusion

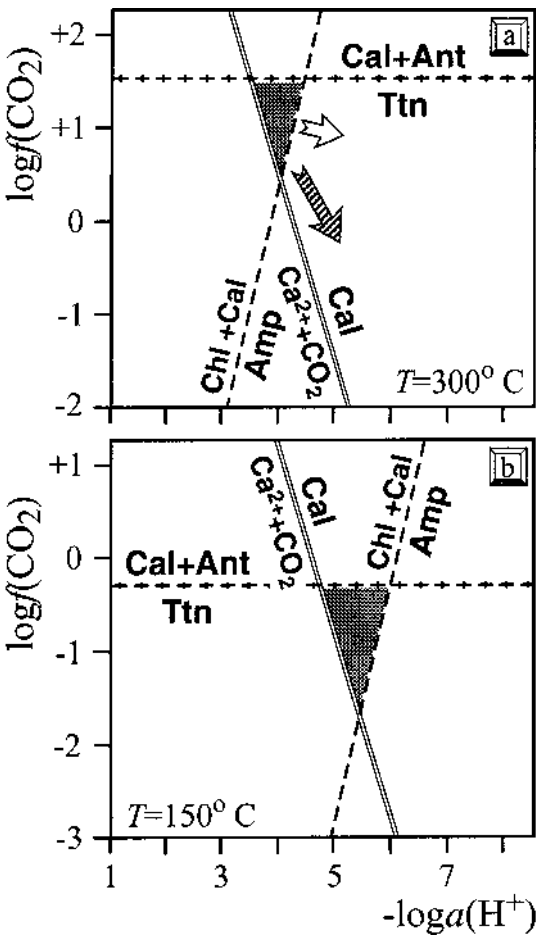

FIG. 12. Phase relationships for the principal late-stage minerals from CAPR relative to $\log f(CO_2)$ and $-\log a(H^+)$ for T = 300°C (a) and 150°C (b). The stippled field corresponds to the conditions at which calcite (Cal), clinochlore (Chl) and titanite (Ttn) coexist in equilibrium. Other symbols: Amp: magnesiohastingsite, Ant: anatase. Empty arrow shows how the Chl + Cal ⇔ Amp equilibrium is affected by increasing $a(Al^{3+})$ or decreasing $a(H_4SiO_4^0)$. Arrow shows how the position of the stippled field changes with decreasing temperature. The Chl + Cal ⇔ Amp equilibrium was calculated for $a(Na^+) = 10^{-3}$.

agrees with the oscillatory variations in Fe/(Fe + Mg) exhibited by spherulitic chlorite from CAPR (Figs. 9, 11a).

The latest association of silicate minerals to crystallize includes the zeolites, muscovite and prehnite. Chemically, it is distinct from the calcite – chlorite – titanite paragenesis in being Na–Al-rich and depleted in Mg and Fe. We consider it unlikely that carbonatitic magma could fractionate a highly polymerized Al–Si-rich fluid. On the other hand, foidolitic rocks (primarily, pegmatites) found in the vicinity of CAPR could be the source of such fluid. Note that nepheline in these rocks is pervasively altered to zeolites and muscovite, and hydrothermal prehnite also occurs in this environment (Kukharenko *et al.* 1965).

The well-documented textural relationships among the late-stage silicate minerals (see Figs. 1, 7, 8c, 9, 11) and our previously published findings (Chakhmouradian & Zaitsev 1999, Zaitsev & Chakhmouradian 2002) were used to construct a generalized paragenetic diagram (Fig. 13). This figure shows the sequence of crystallization of the silicate phases in CAPR, and their temporal

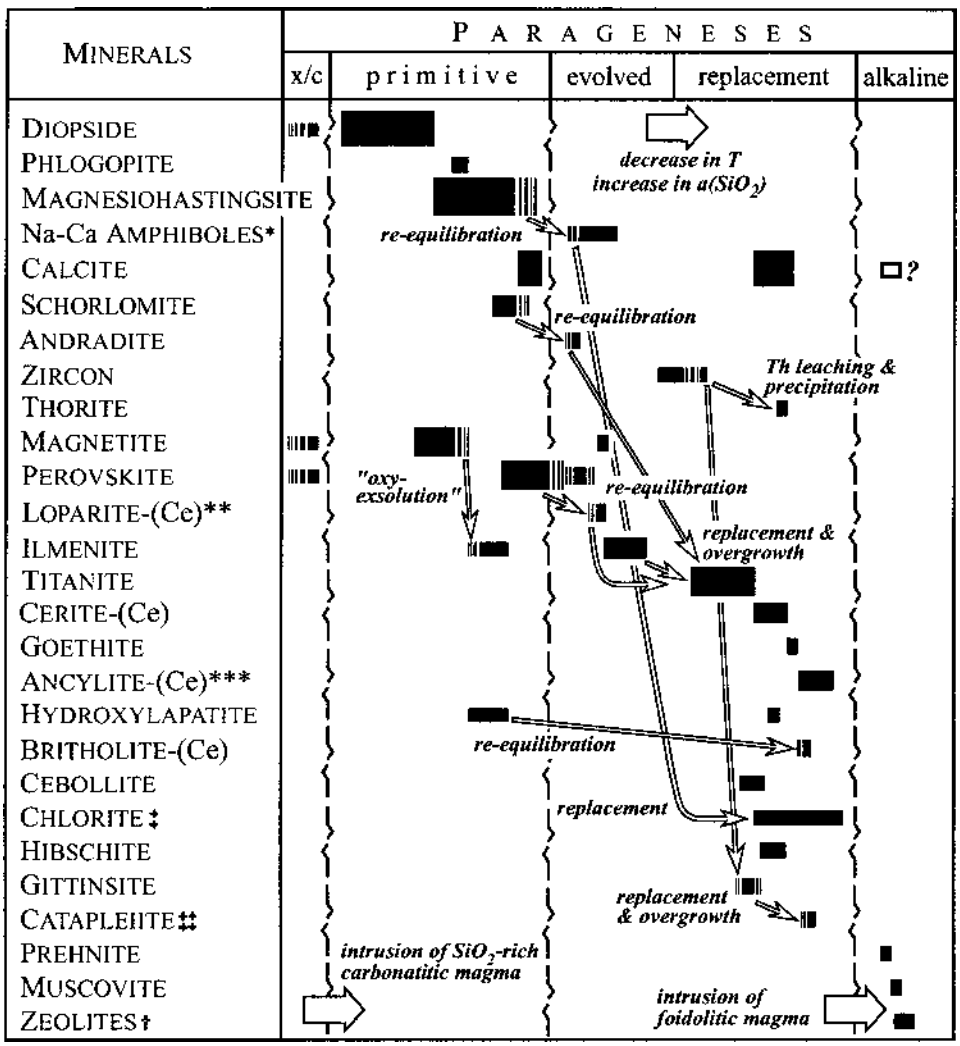

FIG. 13. Generalized paragenetic bar diagram for the calcite – amphibole – clinopyroxene rock from Afrikanda. For details see text. Comments: * richterite and magnesiokatophorite; ** calcian niobian, niobian calcian and thorian niobian loparite-(Ce) and ceroan lueshite; *** ancylite-(Ce) and calcio-ancylite-(Ce); ‡ clinochlore and chamosite; ‡‡ catapleiite and calcium catapleiite; † natrolite, edingtonite and an unidentified Na–Ca–Sr zeolite.

and paragenetic relationships with the principal oxide and oxysalt phases.

Calcite pockets in mafic rocks: an example of mineralogical convergence

Mineral assemblages superficially similar to CAPR occur in deuterically altered mafic and, to a lesser extent, ultramafic rocks. In the latter, successive replacement of clinopyroxene by calcic amphiboles ("hornblende") and clinochlore, followed by precipitation of calcite, produces textures akin to those observed at Afrikanda (Fig. 14). This similarity is even more striking where precursor Ti minerals (especially ilmenite) become replaced by titanite. Evidently, the mineral reactions discussed above are also valid for silica-undersaturated

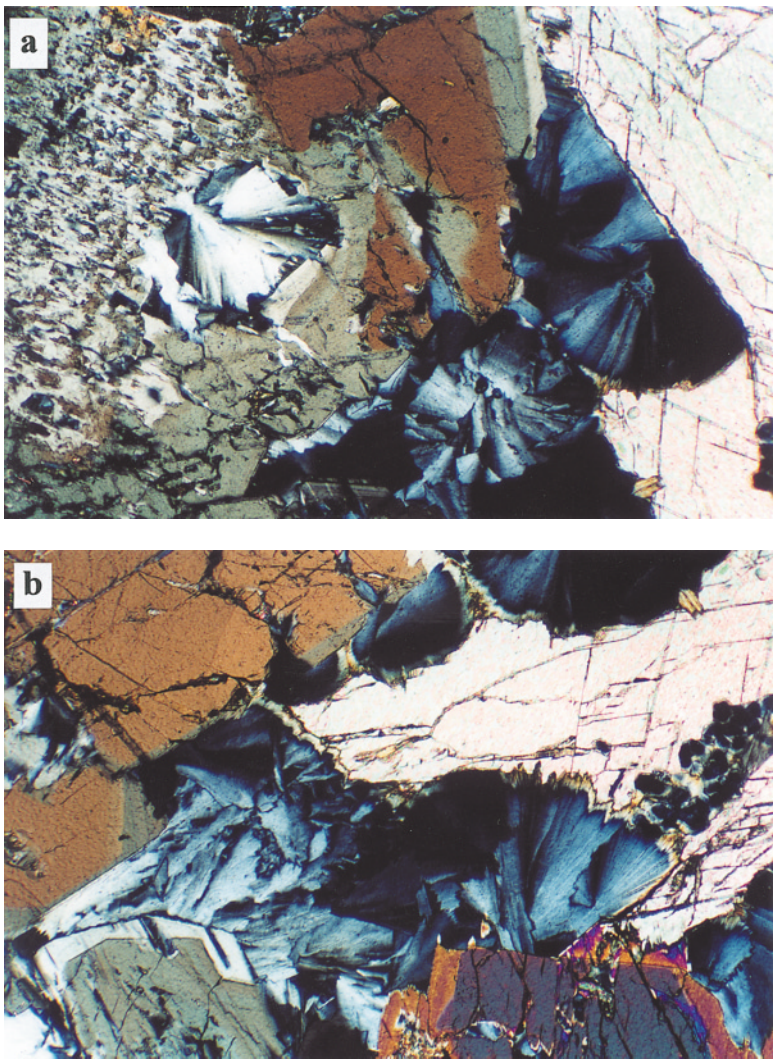

FIG. 14. Photomicrographs of deuterically altered gabbro, Coldwell complex, Ontario (crossed polars; width of the field of view is 5.5 mm for both images). (a) Diopside (left upper corner) replaced and mantled by zoned magnesiohastingsite (brown to olive-green); note spherulites of clinochlore (low interference-colors) at the contact between the amphibole and calcite (pinkish white); (b) zoned crystals of magnesiohastingsite–hastingsite (brown, olive-green and purplish blue) partly replaced and overgrown by clinochlore at the contact with calcite (pinkish white).

rocks lacking any affinity with carbonatites. It should be noted here that Kukharenko *et al.* (1965) interpreted CAPR as the product of "autometasomatic" reactions between the ultramafic suite and a deuteric CO_2-rich fluid. However, a detailed analysis of the compositional characteristics of major and accessory minerals reveals some fundamental differences between CAPR and calcite pockets in mafic rocks.

In the latter, a calcic amphibole is typically accompanied by biotite, both of which commonly contain detectable Cl. The two minerals may not be intimately associated, but are usually present in comparable quantities. Magnesiohastingsite, pargasite and other types of "hornblende" from carbonated mafic rocks show normal zoning toward Fe-enriched compositions, although it is noteworthy that, in common with CAPR, this zoning commonly involves a decrease in K and Ti contents. Deuteric fluids associated with mafic and ultramafic rocks are not sufficiently rich in alkalis to produce sodic–calcic amphiboles like those found in carbonatites (Fig. 5). Calcite from the pockets (Fig. 14b) lacks detectable Sr, whereas titanite found in the same assemblage (not shown) is much poorer in Zr, Nb and *LREE* relative to the Afrikanda titanite (Table 3). Another fundamental difference lies in the assemblage of accessory minerals: that from CAPR comprises an astonishing diversity of Zr, Th, Nb, *REE* and Sr minerals, most of which have never been reported from "carbonated" silica-undersaturated rocks. An extensive search of the literature has shown that the only known occurrence of mafic rocks containing minor amounts of late-stage calcite, associated with ancylite-(Ce) and the Ca zirconosilicate loudounite, is the Goose Creek diabase in Virginia (Dunn & Newberry 1983). Although there have been numerous accounts of accessory zirconolite and baddeleyite in mafic and ultramafic rocks (for review, see Williams & Gieré 1993), these minerals normally crystallize from intercumulus Zr-rich liquids and, to our knowledge, have not been observed in late-stage calcite-bearing parageneses.

The outlined differences clearly demonstrate that the calcite – amphibole – clinopyroxene rock from Afrikanda and deuterically altered mafic (or ultramafic) rocks are merely examples of partial mineralogical convergence. By analogy with biological convergence, the latter may be defined as the response of different mineral assemblages (rocks) to similar physical or chemical processes in the geological environment.

Conclusions

The calcite – amphibole – clinopyroxene rock from Afrikanda is the product of crystallization of an alkali- and silica-rich carbonatitic magma that intruded earlier-formed cumulate ultramafic rocks. CAPR may be classified as "silicocarbonatite". Although this term has been excluded from the classification of igneous rocks approved by the IUGS (Streckeisen 1978), it still widely used to describe rocks that have unquestionable genetic affinities with *bona fide* carbonatites, but exhibit the preponderance of silicate minerals over carbonates in the modal composition. At Afrikanda, the melts parental to the ultramafic suite were not related to the carbonatitic magma by simple fractionation. On the basis of the mineralogical data presented here and in our previous studies (Chakhmouradian & Zaitsev 1999, Zaitsev & Chakhmouradian 2002), we also rule out the possibility that CAPR was produced by deuteric alteration of the cumulate clinopyroxenite.

Solidification of the alkali- and silica-rich carbonatitic magma and associated processes (assimilation of xenocrysts, fractionation of a Na-rich fluid and, to some degree, reaction with the wallrocks) led to the formation of at least three different parageneses that together comprise over 50 mineral species. Enrichment of the magma in Zr, Th, Nb, *REE* and Sr resulted in the crystallization of minerals characteristic of carbonatites (including such silicates as Hf-poor zircon, Zr-bearing schorlomite and catapleiite), as well as several rare minerals that have not been previously reported from carbonatitic rocks (*e.g.*, gittinsite). The latest mineral paragenesis to crystallize consists of alkali aluminosilicates and prehnite, all of which probably precipitated from a fluid derived from younger intrusions of foidolitic magma.

Acknowledgements

This study could not have been accomplished without the generous permission of Roger H. Mitchell and Allan J. MacKenzie to use the instrumental facility at Lakehead University for the analytical work. The help of Ron Chapman with WDS microprobe analyses is also gratefully acknowledged. The manuscript greatly benefitted from the comments and suggestions made by John Gittins, Donald D. Hogarth and Editor Robert F. Martin. Anthony N. Mariano is thanked for sharing his unpublished data on the occurrences of gittinsite in alkaline rocks. The present work was supported by the Natural Sciences and Engineering Research Council of Canada, and the University of Manitoba (ARC).

References

Amelin, Yu. & Zaitsev, A.N. (2002): Precise geochronology of phoscorites and carbonatites: the critical role of U-series disequilibrium in age interpretations. *Geochim. Cosmochim. Acta* **66**, 2399-2419.

Amthauer, G., Annersten, H. & Hafner, S.S. (1977): The Mössbauer spectrum of ^{57}Fe in titanium-bearing andradites. *Phys. Chem. Minerals* **1**, 399-413.

Andersen, T. (1988): Evolution of peralkaline calcite carbonatite magma in the Fen complex, southeast Norway. *Lithos* **22**, 99-112.

_____ (1989): Carbonatite-related contact metasomatism in the Fen complex, Norway: effects and petrogenetic implications. *Mineral. Mag.* **53**, 395-414.

ANSELL, H.G., ROBERTS, A.C., PLANT, A.G. & STURMAN, B.D. (1980): Gittinsite, a new calcium zirconium silicate from the Kipawa agpaitic syenite complex, Quebec. *Can. Mineral.* **18**, 201-203.

ARMBRUSTER, T. (1995): Structure refinement of hydrous andradite, $Ca_3Fe_{1.54}Mn_{0.20}Al_{0.26}(SiO_4)_{1.65}(O_4H_4)_{1.35}$ from the Wessels mine, Kalahari manganese field, South Africa. *Eur. J. Mineral.* **7**, 1221-1225.

_____, BIRRER, J., LIBOWITZKY, E. & BERAN, A. (1998): Crystal chemistry of Ti-bearing andradites. *Eur. J. Mineral.* **10**, 907-921.

BAGDASAROV, YU.A. (1994): On relationships between pyroxene and olivine rocks from the "ore complex" of the Yraas massif, and some peculiarities of their genesis. *Zap. Vser. Mineral. Obshchest.* **123**(1), 50-58 (in Russ.).

BASU, N.K. & MAYILA, A. (1986): Petrographic and chemical characteristics of the Panda Hill carbonatite complex, Tanzania. *J. Afr. Earth Sci.* **5**, 589-598.

BIRKETT, T.C., MILLER, R.R., ROBERTS, A.C. & MARIANO, A.N. (1992): Zirconium-bearing minerals of the Strange Lake intrusive complex, Quebec–Labrador. *Can. Mineral.* **30**, 191-205.

BRIGATTI, M.F., MEDICI, L., SACCANI, E. & VACCARO, C. (1996): Crystal chemistry and petrologic significance of Fe^{3+}-rich phlogopite from the Tapira carbonatite complex, Brazil. *Am. Mineral.* **81**, 913-927.

BULAKH, A.G. & IVANIKOV, V.V. (1984): *Problems in the Mineralogy and Petrology of Carbonatites*. Leningrad Univ. Press, Leningrad, Russia (in Russ.).

CATHELINEAU, M. (1988): Cation site occupancy in chlorites and illites as a function of temperature. *Clay Minerals* **23**, 471-485.

CHAKHMOURADIAN, A.R. & MITCHELL, R.H. (1999): Primary, agpaitic and deuteric stages in the evolution of accessory Sr, REE, Ba and Nb-mineralization in nepheline-syenite pegmatites at Pegmatite Peak, Bearpaw Mts, Montana. *Mineral. Petrol.* **67**, 85-110.

_____ & _____ (2002): The mineralogy of Ba- and Zr-rich alkaline pegmatites from Gordon Butte, Crazy Mountains (Montana, USA): comparisons between potassic and sodic agpaitic pegmatites. *Contrib. Mineral. Petrol.* **143**, 93-114.

_____ & ZAITSEV, A.N. (1999): Calcite – amphibole – clinopyroxene rock from the Afrikanda complex, Kola Peninsula, Russia: mineralogy and a possible link to carbonatites. I. Oxide minerals. *Can. Mineral.* **37**, 177-198.

CURRIE, K.L., KNUTSON, J. & TEMBY, P.A. (1992): The Mud Tank carbonatite complex, central Australia – an example of metasomatism at mid-crustal levels. *Contrib. Mineral. Petrol.* **109**, 326-339.

DAWSON, J.B., SMITH, J.V. & STEELE, I.M. (1995): Petrology and mineral chemistry of plutonic igneous xenoliths from the carbonatite volcano, Oldoinyo Lengai, Tanzania. *J. Petrol.* **36**, 797-826.

DELLA VENTURA, G., BELLATRECCIA, F. & WILLIAMS, C.T. (1999): Zr- and *LREE*-rich titanite from Tre Croci, Vico Volcanic complex (Latium, Italy). *Mineral. Mag.* **63**, 123-130.

DINGWELL, D.B. & BREARLEY, M. (1985): Mineral chemistry of igneous melanite garnets from analcite-bearing volcanic rocks, Alberta, Canada. *Contrib. Mineral. Petrol.* **90**, 29-35.

DUNN, P.J. & NEWBERRY, D. (1983): Loudounite, a new zirconium silicate from Virginia. *Can. Mineral.* **21**, 37-40.

EGOROV, L.S. (1991): *Ijolite–Carbonatite Plutonism.* Nedra, Leningrad, Russia (in Russ.).

FLOHR, M.J.K. & ROSS, M. (1989): Alkaline igneous rocks of Magnet Cove, Arkansas: metasomatized ijolite xenoliths from Diamond Jo quarry. *Am. Mineral.* **74**, 113-131.

FÖRSTER, H.-J. (2000): Cerite-(Ce) and thorian synchysite-(Ce) from the Niederbobritzsch granite, Erzgebirge, Germany: implications for the differential mobility of the *LREE* and Th during alteration. *Can. Mineral.* **38**, 67-79.

GAMBLE, R.P. & TAYLOR, L.A. (1980): Crystal/liquid partitioning in augite: effects of cooling rate. *Earth Planet. Sci. Lett.* **47**, 21-33.

GASPAR, J.C. & WYLLIE, P.J. (1982): Barium phlogopite from the Jacupiranga carbonatite, Brazil. *Am. Mineral.* **67**, 997-1000.

GIANNETTI, B. & LUHR, F. (1983): The white trachytic tuff of Roccamonfina Volcano (Rome Region, Italy). *Contrib. Mineral. Petrol.* **84**, 235-252.

GILBERT, M.C., HELZ, R.T., POPP, R.K. & SPEAR, F.S. (1982): Experimental studies of amphibole stability. *In* Amphiboles: Petrology and Experimental Phase Relations (D.R. Veblen & P.H. Ribbe, eds.). *Rev. Mineral.* **9B**, 229-353.

GITTINS, J., ALLEN, C.R. & COOPER, A.F. (1975): Phlogopitization of pyroxenite; its bearing on the composition of carbonatite magmas. *Geol. Mag.* **112**, 503-507.

GLASS, J.J., EVANS, H.T., JR., CARRON, M.K. & HILDEBRAND, F.A. (1958): Cerite from Mountain Pass, San Bernardino County, California. *Am. Mineral.* **43**, 460-475.

HEAMAN, L.M., BOWINS, R. & CROCKET, J. (1990): The chemical composition of igneous zircon suites: implications for geochemical tracer studies. *Geochim. Cosmochim. Acta* **54**, 1597-1607.

HEATHCOTE, R.C. & MCCORMICK, G.R. (1989): Major-cation substitution in phlogopite and evolution of carbonatite in the Potash Sulphur Springs complex, Garland County, Arkansas. *Am. Mineral.* **74**, 132-140.

HENMI, C., KUSACHI, I. & HENMI, K. (1995): Morimotoite, $Ca_3TiFe^{2+}Si_3O_{12}$, a new titanian garnet from Fuka, Okayama Prefecture, Japan. *Mineral. Mag.* **59**, 115-120.

HILLIER, S. & VELDE, B. (1991): Octahedral occupancy and the chemical composition of diagenetic (low-temperature) chlorites. *Clay Minerals* **26**, 149-168.

HOGARTH, D.D. (1989): Pyrochlore, apatite and amphibole: distinctive minerals in carbonatite. *In* Carbonatites: Genesis and Evolution (K. Bell, ed.). Unwin Hyman, London, U.K. (105-148).

_____, CHAO, G.Y. & TOWNSEND, M.G. (1987): Potassium- and fluorine-rich amphiboles from the Gatineau area, Quebec. *Can. Mineral.* **25**, 739-753.

_____, RUSHFORTH, P. & MCCORKELL, R.H. (1988): The Blackburn carbonatites, near Ottawa, Ontario: dykes with fluidized emplacement. *Can. Mineral.* **26**, 377-390.

HOLLAND, T.J.B. & REDFERN, S.A.T. (1997): Unit cell refinement from powder diffraction data: the use of regression diagnostics. *Mineral. Mag.* **61**, 65-77.

_____ & RICHARDSON, S.W. (1979): Amphibole zonation in metabasites as a guide to the evolution of metamorphic conditions. *Contrib. Mineral. Petrol.* **70**, 143-148.

HORVÁTH, L. & GAULT, R.A. (1990): The mineralogy of Mont Saint-Hilaire, Quebec. *Mineral. Rec.* **21**, 281-359.

HOWIE, R.A. & WOOLLEY, A.R. (1968): The role of titanium and the effect of TiO_2 on the cell-size, refractive index, and specific gravity in the andradite – melanite – schorlomite series. *Mineral. Mag.* **36**, 775-790.

HUGHES, J.M., BLOODAXE, E.S., HANCHAR, J.M. & FOORD, E.E. (1997): Incorporation of rare earth elements in titanite: stabilization of the *A*2/*a* dimorph by creation of antiphase boundaries. *Am. Mineral.* **82**, 512-516.

KAPUSTIN, YU.L. (1971): *Mineralogy of Carbonatites*. Nauka Press, Moscow, Russia (in Russ.).

_____ (1989): Cerite and törnebohmite from fenites of the Tuva alkaline massifs. *Zap. Vses. Mineral. Obshchest.* **118**(4), 47-55 (in Russ.).

KOUCHI, A., SUGAWARA, Y., KASHIMA, K. & SUNAGAWA, I. (1983): Laboratory growth of sector-zoned clinopyroxenes in the system $CaMgSi_2O_6$–$CaTiAl_2O_6$. *Contrib. Mineral. Petrol.* **83**, 177-184.

KOVALENKO, V.I., TSARYEVA, G.M., GOREGLYAD, A.V., YARMOLYUK, V.V., TROITSKY, V.A., HERVIG, R.L. & FARMER, G.L. (1995): The peralkaline granite-related Khaldzan–Buregtey rare metal (Zr, Nb, REE) deposit, western Mongolia. *Econ. Geol.* **90**, 530-547.

KOZYREVA, L.V., SUBBOTINA, G.F. & SUBBOTIN, V.V. (1990): Zircon from Paleozoic alkaline complexes of the Kola Peninsula. *In* Shchelochnoi Magmatism Severo-Vostochnoi Chasti Baltiiskogo Shchita. Kola Science Center Press, Apatity, Russia (88-97; in Russ.).

KRANIDIOTIS, P. & MACLEAN, W.H. (1987): Systematics of chlorite alteration at the Phelps Dodge massive sulfide deposit, Matagami, Quebec. *Econ. Geol.* **82**, 1898-1911.

KRASNOVA, N.I. (2001): The Kovdor phlogopite deposit, Kola Peninsula, Russia. *Can. Mineral.* **39**, 33-44.

KÜHBERGER, A., FEHR, T., HUCKENHOLZ, H.G. & AMTHAUER, G. (1989): Crystal chemistry of a natural schorlomite and Ti-andradites synthesized at different oxygen fugacities. *Phys. Chem. Minerals* **16**, 734-740.

KUKHARENKO, A.A., ORLOVA, M.P., BULAKH, A.G., BAGDASAROV, E.A., RIMSKAYA-KORSAKOVA, O.M., NEFEDOV, E.I., IL'INSKIY, G.A., SERGEEV, A.S. & ABAKUMOVA, N.B. (1965): *The Caledonian Complex of Ultramafic, Alkaline Rocks and Carbonatites of the Kola Peninsula and Northern Karelia*. Nedra Press, Moscow, Russia (in Russ.).

KUPLETSKII, B.M. (1938): The pyroxenite intrusion near Afrikanda station in the Kola Peninsula. *Trudy Petrogr. Inst. Akad. Nauk SSSR* **12**, 71-88 (in Russ.).

LAGER, G.A., ARMBRUSTER, T., ROTELLA, F.J. & ROSSMAN, G.R. (1989): OH substitution in garnets: X-ray and neutron diffraction, infrared, and geometric-modeling studies. *Am. Mineral.* **74**, 840-851.

LARSEN, E.S. & SCHALLER, W.T. (1914): Cebollite, a new mineral. *Wash. Acad. Sci.* **4**(16), 480-482.

LOCOCK, A., LUTH, R.W., CAVELL, R.G., SMITH, D.G.W. & DUKE, M.J.M. (1995): Spectroscopy of the cation distribution in the schorlomite species of garnet. *Am. Mineral.* **80**, 27-38.

LUPINI, L., WILLIAMS, C.T. & WOOLLEY, A.R. (1992): Zr-rich garnet and Zr- and Th-rich perovskite from the Polino carbonatite, Italy. *Mineral. Maj.* **56**, 581-586.

MALITESTA, C., LOSITO, I., SCORDARI, F. & SCHINGARO, E. (1995): XPS investigation of titanium in melanites from Monte Vulture (Italy). *Eur. J. Mineral.* **7**, 847-858.

MCCORMICK, G.R. & HEATHCOTE, R.C. (1987): Mineral chemistry and petrogenesis of carbonatite intrusions, Perry and Conway Counties, Arkansas. *Am. Mineral.* **72**, 59-66.

_____ & LE BAS, M.J. (1996): Phlogopite crystallization in carbonatitic magmas from Uganda. *Can. Mineral.* **34**, 469-478.

MIDDLEMOST, E. (1990): Mineralogy and petrology of the rauhaugites of Mt Weld carbonatite complex of Western Australia. *Mineral. Petrol.* **41**, 145-161.

MITCHELL, R.H. (1980): Pyroxenes of the Fen alkaline complex, Norway. *Am. Mineral.* **65**, 45-54.

MOECHER, D.P., ANDERSON, E.D., COOK, C.A. & MEZGER, K. (1997): The petrogenesis of metamorphosed carbonatites in the Grenville Province, Ontario. *Can. J. Earth Sci.* **34**, 1185-1201.

MOORE, P.B. & SHEN, JINCHUANG (1983): Cerite, $RE_9(Fe^{3+}, Mg)(SiO_4)_6(SiO_3OH)(OH)_3$: its crystal structure and relation to whitlockite. *Am. Mineral.* **68**, 996-1003.

MORBIDELLI, L., BECCALUVA, L., BROTZU, P., CONTE, A., GARBARINO, C., GOMES, C.B., MACCIOTTA, G., RUBERTI, E., SCHEIBE, L.F. & TRAVERSA, G. (1986): Petrological and geochemical studies of alkaline rocks from continental Brazil. 3. Fenitization of jacupirangite by carbonatite magmas in the Jacupiranga Complex, SP. *Per. Mineral.* **55**, 261-295.

MÜNTENER, O. & HERMANN, J. (1994): Titanian andradite in a metapyroxenite layer from the Malenco ultramafics (Italy): implications for Ti-mobility and low oxygen fugacity. *Contrib. Mineral. Petrol.* **116**, 156-168.

OBERTI, R., UNGARETTI, L., CANNILLO, E. & HAWTHORNE, F.C. (1992): The behaviour of Ti in amphiboles. I. Four- and six-coordinate Ti in richterite. *Eur. J. Mineral.* **4**, 425-439.

OTTO, J.W. & WYLLIE, P.J. (1993): Relationships between silicate melts and carbonate-precipitating melts in CaO–MgO–SiO_2–CO_2–H_2O at 2 kbar. *Mineral. Petrol.* **48**, 343-365.

OUZEGANE, K., FOURCADE, S., KIENAST, J.-R. & JAVOY, M. (1988): New carbonatite complexes in the Archean In'Ouzzal nucleus (Ahaggar, Algeria): mineralogical and geochemical data. *Contrib. Mineral. Petrol.* **98**, 277-292.

PAKHOMOVSKY, YA.A., MEN'SHIKOV, YU.P., YAKOVENCHUK, V.N., IVANYUK, G.YU., KRIVOVICHEV, S.V. & BURNS, P.C. (2002): Cerite-(La), $(La,Ce,Ca)_9(Fe,Ca,Mg)(SiO_4)_3[SiO_3(OH)]_4(OH)_3$, a new mineral species from the Khibina alkaline massif: occurrence and crystal structure. *Can. Mineral.* **40**, 1177-1184.

PEKOV, I.V., TURCHKOVA, A.G. & KULIKOVA, I.M. (2001): Barium and potassium zeolites from the Afrikanda alkaline massif (Kola Peninsula). *In* Alkaline Magmatism on Earth. Workshop Proceedings, Moscow, Russia (56-57; in Russ.).

PLATT, R.G. & MITCHELL, R.H. (1979): The Marathon Dikes. I. Zirconium-rich titanian garnets and manganoan magnesian ulvöspinel–magnetite spinels. *Am. Mineral.* **64**, 546-550.

REGUIR, E.P. (2001): *Aspects of the Mineralogy of the Murun Alkaline Complex, Yakutia, Russia*. M.Sc. thesis, Lakehead University, Thunder Bay, Ontario.

ROCK, N.M.S., GWALANI, L.G. & GRIFFIN, B.J. (1994): Alkaline rocks and carbonatites of Amba Dongar and adjacent areas, Deccan Alkaline Province, Gujarat, India. 2. Complexly zoned clinopyroxene phenocrysts. *Mineral. Petrol.* **51**, 113-135.

RUSSELL, J.K., GROAT, L.A. & HALLERAN, A.A.D. (1994): *LREE*-rich niobian titanite from Mount Bisson, British Columbia: chemistry and exchange mechanisms. *Can. Mineral.* **32**, 575-587.

SABINA, A.P. (1964): Rocks and mineral collecting in Canada. 2. Ontario and Quebec. *Geol. Surv. Can., Misc. Rep.* **8**.

SAMOYLOV, V.S. (1977): *Carbonatites: Facies and Formation Conditions*. Nauka Press, Moscow, Russia (in Russ.).

_____ & GORMASHEVA, G.S. (1975): Alkali amphiboles from carbonatites and genetically related rocks. *Zap. Vses. Mineral. Obshchest.* **104**, 145-159 (in Russ.).

SECHER, K. & LARSEN, L.M. (1980): Geology and mineralogy of the Sarfartôq carbonatite complex, southern West Greenland. *Lithos* **13**, 199-212.

SKOSYREVA, M.V., BAGDASAROV, YU.A., VLASOVA, E.V. & ZHUKHLISTOV, A.P. (1988): Typical features of micas from an East European Platform carbonatite deposit (Kursk Magnetic Anomaly region). *Geochem. Int.* **25**(5), 24-34.

STRECKEISEN, A. (1978): Classification and nomenclature of volcanic rocks, lamprophyres, carbonatites and melilitic rocks. *Neues Jahrb. Mineral. Abh.* **134**, 1-14.

TAREEN, J.A.K., VISWANATHIAH, M.N. & KRISHNAMURTHY, K.V. (1980): Hydrothermal synthesis and growth of $Y(OH)CO_3$-ancylite like phase. *Rev. Chim. Minérale* **17**, 50-57.

ULRYCH, J., POVONDRA, P., PIVEC, E., RUTŠEK, J. & SITEK, J. (1994): Compositional evolution of metasomatic garnet in melilitic rocks of the Osečná complex. *Can. Mineral.* **32**, 637-647.

VEKSLER, I.V. & KEPPLER, H. (2000): Partitioning of Mg, Ca, and Na between carbonatite melt and hydrous fluid at 0.1–0.2 GPa. *Contrib. Mineral. Petrol.* **138**, 27-34.

VILADKAR, S.G. & WIMMENAUER, W. (1986): Mineralogy and geochemistry of the Newania carbonatite–fenite complex, Rajasthan, India. *Neues Jahrb. Mineral., Abh.* **156**, 1-21.

VOLOSHIN, A.V., SUBBOTIN, V.V., PAKHOMOVSKIY, YA.A. & MEN'SHIKOV, YU.P. (1989): Sodium zirconosilicates from carbonatites of Vuorijarvi (Kola Peninsula). *Novye Dannye Mineral.* **36**, 3-12 (in Russ.).

WILLIAMS, C.T. & GIERÉ, R. (1993): Zirconolite: a review of localities worldwide, and a compilation of its chemical compositions. *Bull. Nat. Hist. Mus. London* (*Geol.*) **52**, 1-24.

WOOLLEY, A.R., BARR, M.W.C., DIN, V.K., JONES, G.C., WALL, F. & WILLIAMS, C.T. (1991): Extrusive carbonatites from the Uyaynah area, United Arab Emirates. *J. Petrol.* **32**, 1143-1167.

WU, GONGBAO & MU, BAOLEI (1986): The crystal chemistry and Mössbauer study of schorlomite. *Phys. Chem. Minerals* **13**, 198-205.

YODER, H.S., JR. (1975): Relationship of melilite-bearing rocks to kimberlite: a preliminary report on the system akermanite–CO_2. *Phys. Chem. Earth* **9**, 883-894.

YOUNG, B.N., PARSONS, I. & THREADGOULD, R. (1994): Carbonatite near the Loch Borralan intrusion, Assynt. *J. Geol. Soc. London* **151**, 945-954.

ZAITSEV, A.N. (1992): *The Mineralogy of Carbonatites of the Khibina Massif, and Their Major Genetic Features*. Ph.D. thesis, St. Petersburg State University, St. Petersburg, Russia (in Russ.).

_____ & CHAKHMOURADIAN, A.R. (2002): Calcite – amphibole – clinopyroxene rock from the Afrikanda complex, Kola Peninsula, Russia: mineralogy and a possible link to carbonatites. II. Oxysalt minerals. *Can. Mineral.* **40**, 103-120.

_____, SITNIKOVA, M.A., SUBBOTIN, V.V., CHAKHMOURADIAN, A.R., WALL, F. & KRETSER, YU.L. (1999): Nb–Zr mineralization in the Sallanlatvi carbonatites, Kola Peninsula, Russia. *In* Mineral Deposits: Processes to Processing (C.J. Stanley *et al.*, eds.). A.A. Balkema, Rotterdam, The Netherlands (691-694).

ZANE, A., SASSI, R. & GUIDOTTI, C.V. (1998): New data on metamorphic chlorite as a petrogenetic indicator mineral, with special regard to greenschist-facies rocks. *Can. Mineral.* **36**, 713-726.

Received February 1, 2002, revised manuscript accepted September 23, 2002.

APPENDIX

Mineral equilibria discussed in the text:

$$CaTiO_3 + H_4SiO_4^0 \Rightarrow CaTiSiO_5 + 2H_2O \quad (1)$$
Perovskite Titanite

$$FeTiO_3 + Ca^{2+} + H_4SiO_4^0 \Rightarrow CaTiSiO_5 + 2H_2O + Fe^{2+} \quad (2)$$
Ilmenite Titanite

$$5NaCa_2Mg_4FeAl_2Si_6O_{22}(OH)_2 + 34H_2O + 26H^+ + 10CO_2 \Rightarrow$$
Magnesiohastingsite

$$4Mg_5Al_2Si_3O_{10}(OH)_8 + 18H_4SiO_4^0 + 10CaCO_3 + 5Na^+ + 5Fe^{3+} + 2Al^{3+} \quad (3)$$
Clinochlore Calcite

$$CaCO_3 + 2H^+ \Rightarrow Ca^{2+} + CO_2 + H_2O \quad (4)$$
Calcite

$$CaTiSiO_5 + 2H_2O + CO_2 \Rightarrow CaCO_3 + TiO_2 + H_4SiO_4^0 \quad (5)$$
Titanite Calcite Anatase